

AD-A052 068

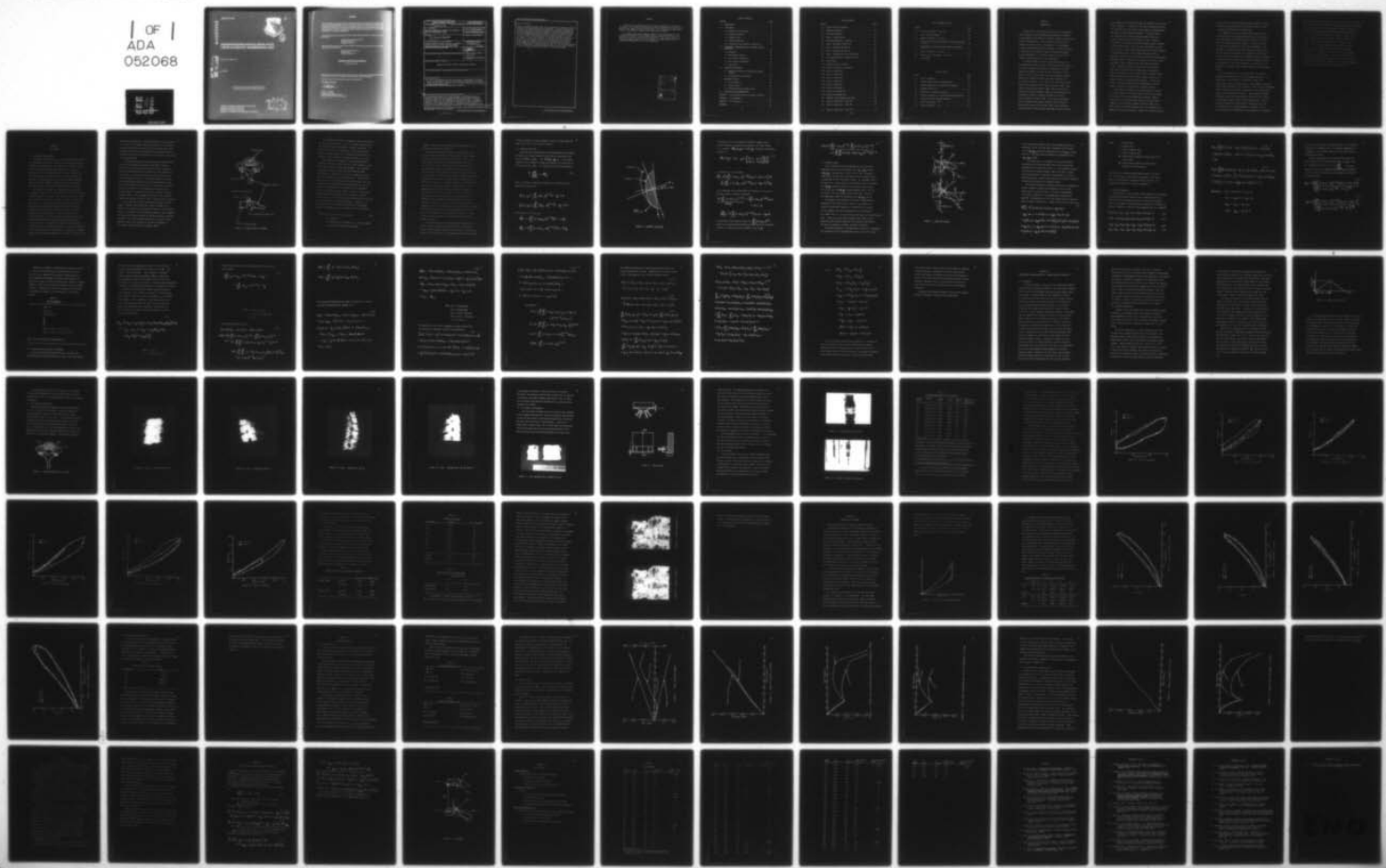
AEROSPACE MEDICAL RESEARCH LAB WRIGHT-PATTERSON AFB OHIO F/G 6/4
NONLINEAR BIOMECHANICAL MODEL OF THE CERVICAL-THORACIC TRANSREG--ETC(U)
JUN 77 W C EDDY

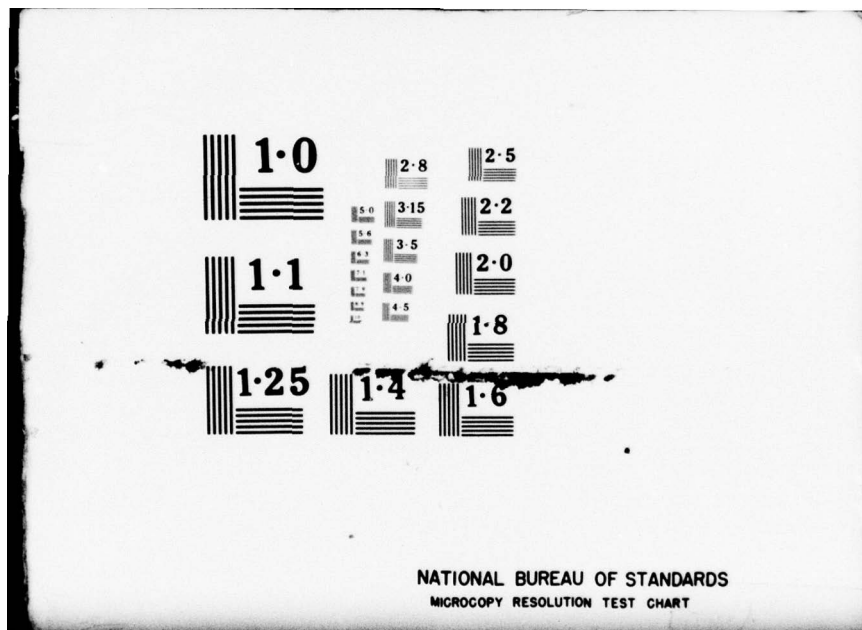
UNCLASSIFIED

AMRL-TR-76-90

NL

| OF |
ADA
052068





NATIONAL BUREAU OF STANDARDS
MICROCOPY RESOLUTION TEST CHART

AMRL-TR-76-90

ADA 052068



1

NONLINEAR BIOMECHANICAL MODEL OF THE CERVICAL-THORACIC TRANSREGIONAL JOINT

WILLIAM C. EDDY, PhD

JUNE 1977

Approved for public release; distribution unlimited

AEROSPACE MEDICAL RESEARCH LABORATORY
AEROSPACE MEDICAL DIVISION
AIR FORCE SYSTEMS COMMAND
WRIGHT-PATTERSON AIR FORCE BASE, OHIO 45433

D D C
REPORT # ED
APR 4 1978
REF ID: A651160
F

NOTICES

When US Government drawings, specifications, or other data are used for any purpose other than a definitely related Government procurement operation, the Government thereby incurs no responsibility nor any obligation whatsoever, and the fact that the Government may have formulated, furnished, or in any way supplied the said drawings, specifications, or other data, is not to be regarded by implication or otherwise, as in any manner licensing the holder or any other person or corporation, or conveying any rights or permission to manufacture, use, or sell any patented invention that may in any way be related thereto.

Please do not request copies of this report from Aerospace Medical Research Laboratory. Additional copies may be purchased from:

**National Technical Information Service
5285 Port Royal Road
Springfield, Virginia 22161**

Federal Government agencies and their contractors registered with Defense Documentation Center should direct requests for copies of this report to:

**Defense Documentation Center
Cameron Station
Alexandria, Virginia 22314**

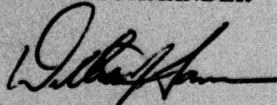
TECHNICAL REVIEW AND APPROVAL

AMRL-TR-76-90

This report has been reviewed by the Information Office (OI) and is releasable to the National Technical Information Service (NTIS). At NTIS, it will be available to the general public, including foreign nations.

This technical report has been reviewed and is approved for publication.

FOR THE COMMANDER



**WILLIAM J. GANNON
Associate Director
Biodynamics and Bionics Division
Aerospace Medical Research Laboratory**

AIR FORCE - 14 JUL 77 - 100

SECURITY CLASSIFICATION OF THIS PAGE (When Data Entered)

REPORT DOCUMENTATION PAGE			READ INSTRUCTIONS BEFORE COMPLETING FORM
1. REPORT NUMBER 14 AMRL-TR-76-90	2. GOVT ACCESSION NO.	3. RECIPIENT'S CATALOG NUMBER	
4. TITLE (and Subtitle) NONLINEAR BIOMECHANICAL MODEL OF THE CERVICAL-THORACIC TRANSREGIONAL JOINT.		5. TYPE OF REPORT & PERIOD COVERED Doctoral Dissertation thesis	
6.		7. PERFORMING ORG. REPORT NUMBER	
7. AUTHOR(s) 14 William C./Eddy, PhD		8. CONTRACT OR GRANT NUMBER(s)	
9. PERFORMING ORGANIZATION NAME AND ADDRESS Aerospace Medical Research Laboratory, Aerospace Medical Division, Air Force Systems Command, Wright-Patterson Air Force Base, Ohio 45433		10. PROGRAM ELEMENT, PROJECT, TASK AREA & WORK UNIT NUMBERS 62202F, 7231-06-56 771461	
11. CONTROLLING OFFICE NAME AND ADDRESS		12. REPORT DATE 11 Jun 77	
14. MONITORING AGENCY NAME & ADDRESS (if different from Controlling Office) 12 194 P.		13. NUMBER OF PAGES 96	
		15. SECURITY CLASS. (of this report) UNCLASSIFIED	
		15a. DECLASSIFICATION/DOWNGRADING SCHEDULE	
16. DISTRIBUTION STATEMENT (of this Report) Approved for public release; distribution unlimited			
17. DISTRIBUTION STATEMENT (of the abstract entered in Block 20, if different from Report)			
18. SUPPLEMENTARY NOTES *Dr. Eddy's postgraduate work with the College of Engineering, University of Denver, was supported by the Air Force Institute of Technology. He worked closely with Dr. Leon E. Kazarian of the Aerospace Medical Research Laboratory, during his experimental work.			
19. KEY WORDS (Continue on reverse side if necessary and identify by block number)			
20. ABSTRACT (Continue on reverse side if necessary and identify by block number) A two dimensional model of the cervical-thoracic transregional joint is developed, which incorporates vertebra geometry and the measured material response properties of the ligaments and intervertebral disc. The model provides a useful tool for the parametric study of the effects of anatomical elements on the overall joint motion. In the model, the joint motion is restricted to the sagittal plane, and the articulating facet surfaces for the adjacent vertebrae are represented by two curves. The requirement that point next page			

DD FORM 1 JAN 73 1473 EDITION OF 1 NOV 65 IS OBSOLETE

SECURITY CLASSIFICATION OF THIS PAGE (When Data Entered)

009850

EB

Block 20. (Cont'd)

contact be maintained between these curves constitutes a kinematic constraint on the relative motion between the two vertebrae. The model considers the vertebrae to be rigid bodies and the masses of the vertebrae are neglected. The characterization of the velocity dependent response of the anterior and posterior longitudinal ligaments is based on a set of experiments in which load versus deflection data were generated at deflection rates of 0.5 and 1 inch per second. From these data, a constitutive equation is derived, consisting of a third order polynomial of the deflection plus a fifth term, the product of an arbitrary constant, the deflection and the deflection velocity. A least squares curve fit of the experimental data is used to obtain values for the arbitrary constants in the constitutive equation. The thirty-one equations resulting from the model are linearized using Newton's method and are solved to provide parametric results for the relative motion of the C7-T1 joint resulting from a given set of input conditions.

PREFACE

This effort was supported by the Air Force Institute of Technology. The report is Dr. Eddy's dissertation in partial fulfillment of the requirement for the degree, Doctor of Philosophy. He performed his postgraduate study in the College of Engineering, University of Denver.

Dr. Eddy's work closely support efforts of the Biodynamics and Bioengineering Division of the Aerospace Medical Research Laboratory, under work unit 7231-06-56, "Spinal Injury Mechanics." He received advice and technical support from Dr. Leon E. Kazarian, the AMRL project officer, during his experimental work in the Laboratory.

ACCESSION for	
NTIS	W 7e Section <input checked="" type="checkbox"/>
DDC	B 7f Section <input type="checkbox"/>
UNANNOUNCED	<input type="checkbox"/>
JUSTIFICATION _____	
BY _____	
DISTRIBUTION/AVAILABILITY CODES	
DIST	SP. CIAL
A	

TABLE OF CONTENTS

CHAPTER	PAGE
I. INTRODUCTION	1
II. JOINT MODEL	5
2.1 Anatomical Considerations	5
2.2 Kinematic Constraint	10
2.3 Kinematic Model	13
2.4 Governing Equations	16
2.5 Linearization and Solution of Equations	19
III. EXPERIMENTAL CHARACTERIZATION OF LIGAMENT MATERIAL PROPERTIES	29
3.1 Background	29
3.2 Experimental Approach	30
3.3 Test Specimen Preparation	33
3.4 Test Fixture and Equipment	38
3.5 Test Results.	40
IV. CONSTITUTIVE EQUATIONS	55
4.1 Anterior and Posterior Longitudinal Ligament Response.	55
4.2 Intervertebral Disc Response.	62
V. PARAMETRIC RESULTS	64
5.1 Initial Solution	64
5.2 Velocity Effect	66
5.3 Articulating Facet Geometry Effect	71
VI. CONCLUSIONS AND RECOMMENDATIONS	75
APPENDIX A. Vector Between Points on Adjacent Vertebrae . .	77
APPENDIX B. Test Equipment.	80
APPENDIX C. Test Parameters	81
REFERENCES	85

LIST OF FIGURES

FIGURE	PAGE
2.1 Seventh Cervical Vertebra	7
2.2 Kinematic Constraint	11
2.3 Free Body Diagram	14
3.1 Shape of Loading Pulse	32
3.2 Specimen Preparation - Saw Cuts	33
3.3 X-Ray - Speciment 11X and 12X	34
3.4 X-Ray - Specimen 13X and 14X	35
3.5 X-Ray - Specimen 15X and 17X	36
3.6 X-Ray - Specimen 18X, 19X, 20X and 21X	37
3.7 Test Specimen Prior to Removal of Disc	38
3.8 Test Fixture	39
3.9 Specimen Loaded in Fixture	41
3.10 Fixture in Tensile Test Machine	41
3.11 Load vs. Deflection	44
3.12 Load vs. Deflection	45
3.13 Load vs. Deflection	46
3.14 Load vs. Deflection	47
3.15 Load vs. Deflection	48
3.16 Load vs. Deflection	49
3.17 Failure in Specimen 11X	53
3.18 Failure in Specimen 11X	53
4.1 Response to Rectangular Load Pulse	56
4.2 Load vs. Deflection - Test 184	58
4.3 Load vs. Deflection - Test 185	59
4.4 Load vs. Deflection - Test 173	60

LIST OF FIGURES (Cont'd)

FIGURE	PAGE
4.5 Load vs. Deflection - Test 175	61
5.1 Input Loads and Moments	67
5.2 Angle of Rotation: -22° Case	68
5.3 Contact Point Coordinates Without Velocity Dependence: -22° Case	69
5.4 Contact Point Coordinates With Velocity Dependence: -22° Case	70
5.5 Angle of Rotation: -35° Case	72
5.6 Contact Point Coordinates: -35° Case	73
A.1 Vector \vec{R}_{mn}^{lk}	79

LIST OF TABLES

TABLE	PAGE
2.1 List of Variables.	19
3.1 Specimen Identification and Dimensions	42
3.2 Average Dimensions for Longitudinal Ligaments	50
3.3 Ligament Yield Loads	51
3.4 Comparison of Average Yield Loads	51
4.1 Arbitrary Constants for Ligament Response Functions. .	57
4.2 Constants for Disc Response Function	62
5.1 Initial Conditions: -22°	65
5.2 Initial Conditions: -35°	65

CHAPTER I
INTRODUCTION

During the past fifteen years, there has been considerable effort expended to apply engineering knowledge and techniques to investigate the functions of biological systems and specifically those of the human body. This work spans the spectrum from attempts to improve athletic performance to the development of highly sophisticated medical technology. The work described in this paper is an attempt to apply an engineering approach to the investigation of the dynamic response of the cervical-thoracic transregional joint of the human spine.

The spinal column has received significant attention in the biomechanical area due to the seriousness and high incidence of injuries resulting from athletic, automobile and military operational accidents and from aircraft ejections by military pilots. Efforts have been made to measure mechanical response during tests using both cadavers and human volunteers such as the work by Clarke et al. (1971), Mertz and Patrick (1971), Gadd, Culver and Naham (1971), Clemens and Burow (1972), Lange (1971), and Bhalla and Simmons (1969). Other work has been conducted to develop mechanical necks for test simulation such as reported by Melvin, McElboney and Roberts (1972) and Calver, Neathery and Mertz (1972). Still other investigators such as Nachemson (1960, 1963), Kazarian (1972), Kazarian, Boyd, and Von Gierke (1971), Farfan (1969, 1971), Nachemson and Evans (1968), Tkaczuk (1967), and Markolf and Morris (1974)

have attempted to describe and explain the functions of the various spinal components. In addition to the above experimental efforts, the spine has been modeled with varying degrees of sophistication starting with simple mass-spring models, continuous elastic and viscoelastic beam models, lumped-parameter models such as that developed by Toth (1967) using a series of springs and dashpots, and finally the discrete parameter model developed by Orne and Liu (1971). This last model represented the spine with a series of rigid bodies representing the vertebrae separated by viscoelastic discs. A later lumped parameter model was developed by Hopkins (1971), and there have been more sophisticated continuous models developed by Li, Advoni and Lee (1971), Krause and Shirazi (1971), Shirazi (1971), and Rybicki and Hopper (1971). Soechting and Pasley (1973) also used a continuous model but incorporated muscular loads using a viscoelastic model for the muscles, and in another effort to consider muscle loads, Thurston and Fay (1974) used a constant torque in the rotating joints to represent these influences. In this last effort, a mechanical neck was also developed, which included members fabricated from shock cord to simulate muscles.

These models are adequate, in varying degrees, to predict the gross response of the spinal column or neck, and to answer the questions for which the models were designed. However, if one wishes to investigate local response of spinal column components, and to predict failures and failure modes, the above models are inadequate because they do not include local geometry and material properties. Because of a specific interest

on the part of the Aerospace Medical Research Laboratory, Wright-Patterson Air Force Base, Ohio, the following attempt was made to develop a micro-model of the human spine.

The approach is to take a single joint consisting of two vertebrae and the intervening intervertebral disc, incorporate the local geometry and constraints into a kinematic model, and solve the governing equations of motion. Forces are derived from constitutive equations for the disc and ligaments. The vertebrae are treated as rigid bodies since the deformation of the bony material was assumed to be insignificant with respect to that of the viscoelastic disc and ligament material, and motion is restricted to the sagittal plane, therefore keeping the model two dimensional. The latter assumption is not dictated by the approach and the model could be three dimensional with additional effort.

The most difficult part of this approach is to establish constitutive equations for the disc and ligament materials. The complexities of this problem are discussed by Fung (1972) and Kazarian (1972), but there is only a limited amount of material property data published in the literature. There has been considerable effort to describe the function and response of the intervertebral disc and work continues in this area. Data reported by Markolf and Morris (1974) and Yomada and Evans (1970) are used to derive a constitutive equation for use in the present effort. However, material property data (stress-strain, load-deflection, creep or relaxation) on the spinal ligaments is extremely limited, and the data that are available have been generated from specimens

taken only from the lumbar region of the spine. Hence, the experimental program discussed in Chapter III was conducted to produce a minimum amount of load-deflection data from which to develop constitutive equations for the anterior and posterior longitudinal ligaments.

In the following discussions, the model is applied to the lower neck where the spine transitions from the cervical to the thoracic region. This is speculated to be a region of high incidence of Air Force operational injuries (Kazarian, 1974), and there is also a radical change in geometry as described by Gray (1973). In Chapter V, the model is used to investigate the effect of articulate geometry on the joint motion and the distribution of loads between the anterior and posterior column. Limitations of the modeling technique as well as areas of expanded development and application are discussed in Chapter VI.

CHAPTER II

JOINT MODEL

2.1 Anatomical Considerations.

The spinal column consists of 24 articulated vertebrae separated by intervertebral discs, and constitutes the primary load-carrying structure of the human body. The motion of the vertebral column, as well as that between individual vertebrae, is a function of external loads, the vertebrae geometry, the load transmitted by the discs, and the loads exerted on the column by ligaments and muscles. Of particular interest here are the vertebrae geometry, the disc and major ligaments associated with the joint between the seventh cervical (C7) and the first thoracic (T1) vertebrae.

The vertebra is composed of a cancellous bone material and its geometry changes with the spinal level. Fig 2.1 shows a typical vertebra from the C7-T1 region. The vertebra is made up of a body and the posterior arch which is joined to the body on either side by a pedicle. At the junction of the arch and the pedicles are the superior and inferior articulating facets, which when mated respectively with the inferior and superior facets of adjacent vertebrae, form synovial joints. In the cervical spine, the articulating facets of a given vertebra are joined by well defined columns which also form the junction between the pedicles and the posterior arch. The respective orientations of the superior and inferior facets are cranial and caudal. As the spine transitions to the thoracic region, the facets change to a posterior - anterior orientation, and the column between the two tends to flatten out and

becomes less well defined. Projecting dorsally from the centerline of the arch is the spinous process, and there are two transverse processes which project laterally from the vertebral body. These latter processes affect lateral motion and are not given further consideration here since the motion of the model will be restricted to the sagital plane.

The vertebral bodies are bound together by the intervertebral disc, and the anterior and posterior longitudinal ligaments. The discs are not unique in the different levels of the spine, as are the vertebrae, except for their size. Four elements make up each disc: the annulus fibrosus, the nucleus pulposus, and two cartiliginous end plates. The annulus fibrosus is a series of fibrocartiliginous bands, which run circumferentially around the disc and encloses the soft nucleus. The bands of the annulus attach top and bottom to the cartiliginous end plates, which in turn attach to the inferior and superior surfaces of adjacent vertebrae bodies. This arrangement constitutes a load carrying element, the rheology of which is still a subject of much discussion.

The anterior and posterior longitudinal ligaments are long bands of fibrous tissue which extend along the length of the spine and are attached to the respective surfaces of the vertebral bodies. In addition to the longitudinal ligaments, other ligaments tie together the posterior arches and spinous processes of adjacent vertebrae. For a more detailed discription of the spinal column anatomy as well as the functions of the various elements see Gray (1973), Kazarian (1972) and Ingemark (1959).

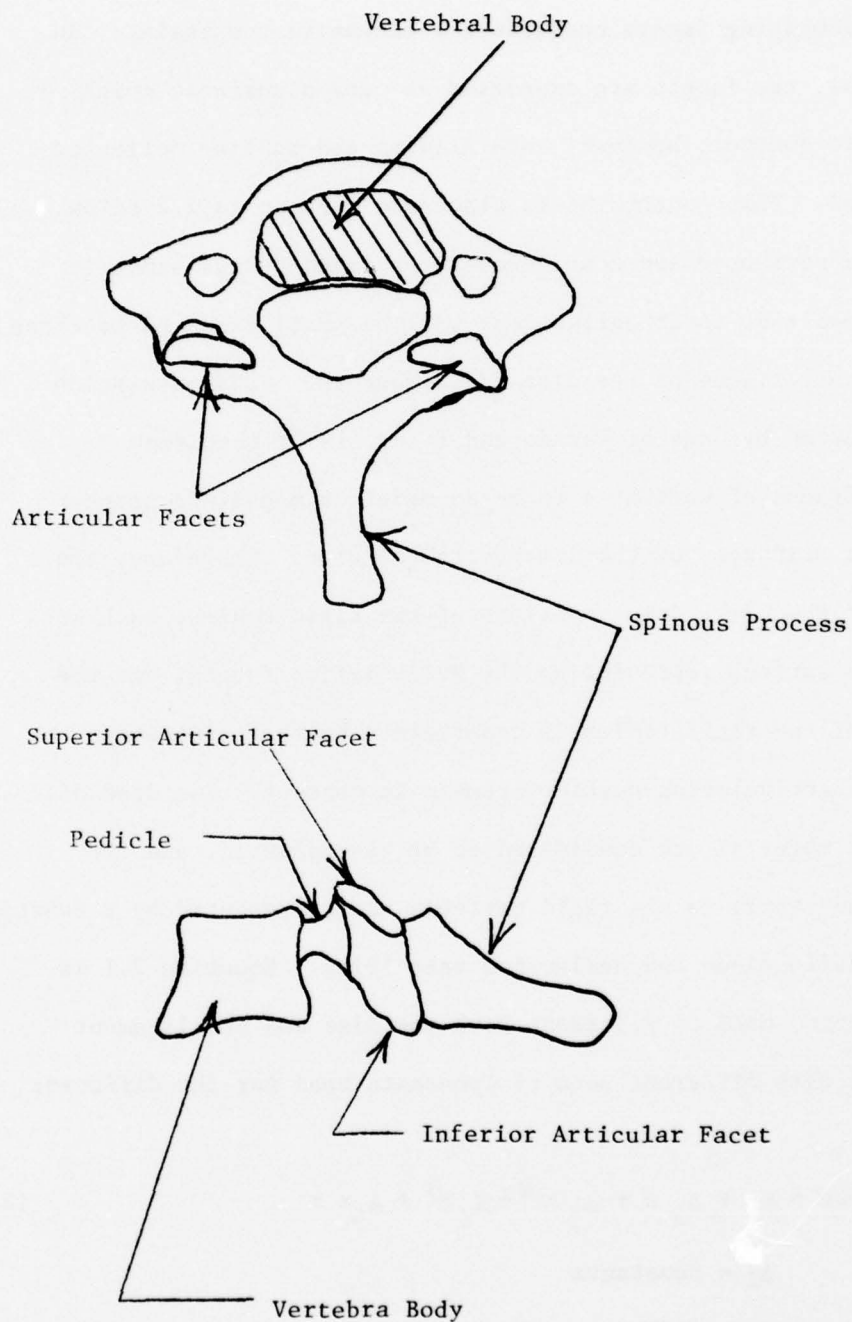


FIGURE 2.1 - SEVENTH CERVICAL VERTEBRA

In formulating the model, an attempt was made to incorporate the anatomy discussed above. The first assumption made was that the articulating facets constitute a kinematic constraint. In the model, the facets are expressed as curved surfaces which remain in contact; however, both sliding and rolling motion is permitted. This constraint is discussed further in 2.2 below.

The vertebrae are considered to be rigid bodies since it is assumed that their deflections will be small compared to those of the soft tissue of the disc and ligaments. This assumption is supported by data of Yamada and Evans (1970) that show the stiffness of vertebrae to be an order of magnitude greater than the stiffness of the intervertebral disc. Therefore, the model of the C7-T1 joint consists of two rigid bodies, each with a curved surface representing the articulating facets, and the motion of the rigid bodies is constrained by the requirement that the articulating surfaces remain in contact. The disc and ligament material are considered to be viscoelastic, and the loads they apply to the rigid vertebra are represented by a function of the deflections and deflection velocities. Equation 2.1 is the function used to represent both the disc and the ligament material with different sets of constants used for the different

$$\text{Force} = A_1 + A_2 x + A_3 x^2 + A_4 x^3 + A_5 x \dot{x} \quad (2.1)$$

A_i = constants

x = deflection of the element, i.e., disc or ligament

\dot{x} = deflection velocity of the element

elements. The choice of this function and the selection of the constants is discussed in Chapter IV.

One further assumption was made in formulating the model. The mass of the joint itself was considered to be small compared to that of the head and neck above the C7 level. Liu et al. (1971) report the mass of a slice taken through the neck at the C7-T1 level to be $0.00348 \text{ lb-sec}^2/\text{in}$, and the mass of the neck above that level to be $0.00833 \text{ lb-sec}^2/\text{in}$. The mass of the C7-T1 slice includes that of all the soft tissue of the neck as well as that of vertebral column segment, and the author reports distortion of the cadaver which would cause the results of the C7-T1 slice to be high. In addition, Clauser et al. (1969) reports head masses to range from 0.0214 to $0.0305 \text{ lb-sec}^2/\text{in}$. These figures support the above assumption, and hence, the mass of the joint is neglected in the model. The inertial effects of the head and neck are included, however, when inputting forces and moments into the rigid body representing the C7 vertebra. Therefore, the model is static at any point in time, but the response at that time is dependent on the inertial effects included in the model inputs, and on the response history prior to that time. The dependence on the prior response history is a result of the viscoelastic nature of the intervertebral disc and the various ligaments.

The following sections of this chapter show the derivation of the kinematic constraint associated with the articulating facets, and the governing equations for the model. The resulting equations are nonlinear due to the geometry and material responses,

so Newton's method is used to generate a series of linear equations which can be solved in an iterative process.

2.2 Kinematic Constraint.

Since the curves representing the articulating facts must remain in contact, the outward normals to the curves are expressed by the functions $f_1(x_1, y_1)$ and $f_2(x_2, y_2)$; the outward normals can be determined by taking the gradient of the functions as discussed by Wylie (1966). The constraint can then be expressed as:

$$K \frac{\vec{\nabla} f_1}{|\vec{\nabla} f_1|} = \vec{\nabla} f_2 \quad (2.2)$$

where K is constant. Referring to Figure 2.2, the curves are now expressed as polynomials.

$$f_1(x_1, y_1) = \sum_{i=1}^N (a_{1i} x_1^{(i-1)}) - y_1 = 0$$

$$f_2(x_2, y_2) = \sum_{i=1}^M (a_{2i} x_2^{(i-1)}) - y_2 = 0$$

The gradients of f_1 and f_2 are:

$$\vec{\nabla} f_1 = \left(\sum_{i=1}^N (i-1) a_{1i} x_1^{(i-2)} \right) \vec{x}_1 - \vec{f}_1$$

$$\vec{\nabla} f_2 = \left(\sum_{i=1}^M (i-1) a_{2i} x_2^{(i-2)} \right) \vec{x}_2 - \vec{f}_2$$

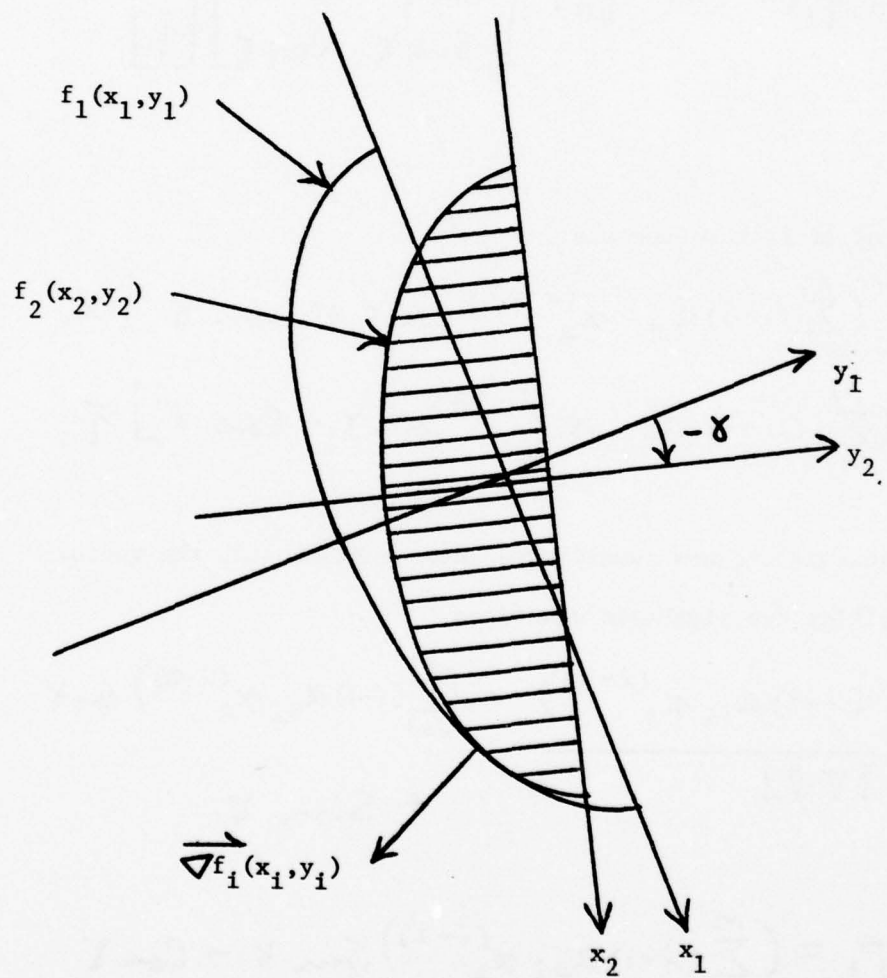


FIGURE 2.2 - KINEMATIC CONSTRAINT

The gradients are in two different coordinate systems, thus it becomes necessary to transform one gradient to the other system,

i.e., transform $\vec{\nabla} f_2(x_2, y_2)$ to the (\vec{x}_1, \vec{y}_1) coordinate system using equation 2.3.

$$\vec{R}(\vec{x}_1, \vec{y}_1) = (x_2 \ y_2) \begin{bmatrix} \cos \gamma & \sin \gamma \\ -\sin \gamma & \cos \gamma \end{bmatrix} \begin{bmatrix} \vec{x}_1 \\ \vec{y}_1 \end{bmatrix} \quad (2.3)$$

The gradient of f_2 then becomes:

$$\begin{aligned} \vec{\nabla} f_2 &= \left[\left(\sum_{i=1}^M (i-1) a_{2i} x_2^{(i-2)} \right) \cos \gamma + \sin \gamma \right] \vec{x}_1 \\ &\quad + \left[\left(\sum_{i=1}^M (i-1) a_{2i} x_2^{(i-2)} \right) \sin \gamma - \cos \gamma \right] \vec{y}_1, \end{aligned}$$

If the gradients are now substituted into equation 2.2, the vector equation yields two algebraic equations.

$$\frac{K \left(\sum_{i=1}^N (i-1) a_{1i} x_1^{(i-2)} \right)}{|\nabla f_1|} = \left(\sum_{i=1}^M (i-1) a_{2i} x_2^{(i-2)} \right) \cos \gamma + \sin \gamma$$

$$\frac{-K}{|\nabla f_1|} = \left(\sum_{i=1}^M (i-1) a_{2i} x_2^{(i-2)} \right) \sin \gamma - \cos \gamma$$

Multiplying the second equation above by $(\sum_{i=1}^N (i-1) a_{1i} x_1^{i-3})$, adding the two equations and dividing by $\cos \gamma$ yields the constraint equation 2.4, which relates the variables x_1, x_2 , and γ .

(2.4)

$$\tan \gamma = \frac{\left(\sum_{i=1}^N (i-1) a_{1i} x_1^{(i-2)} - \sum_{i=1}^M (i-1) a_{2i} x_2^{(i-2)} \right)}{1 + \sum_{i=1}^N \sum_{j=1}^M (i-1)(j-1) a_{1i} a_{2j} x_1^{(i-2)} x_2^{(j-2)}}$$

2.3 Kinematic Model.

Fig 2.3 shows the free body diagrams for the rigid bodies representing the C7 and T1 vertebrae. The (x_{23}, y_{23}) and the (x_{32}, y_{32}) coordinates are fixed to the T1 and C7 vertebrae, respectively, and the curves representing the articulating facets are expressed in these coordinate systems. The angle γ , defined in section 2.2, is the angle of rotation between these two systems.

The (x_2, y_2) coordinate system is the inertial system in which T1 is fixed, and the (x_3, y_3) system translates with C7 but does not rotate. The input moment as well as the input transverse and longitudinal loads are expressed in the (x_3, y_3) system.

The loading of the vertebrae by the disc is simplified and represented by two point loads, F_3 and F_4 . The anterior and posterior longitudinal ligaments are represented by F_5 and F_6 , and the ligament loads on the posterior arch are represented by a single force F_7 . F_8 is the contact load normal to the articulating facet. (Since the facets form a synovial joint, which is well lubricated under healthy conditions, the transverse load between the facets is assumed to be small, and hence is ignored.)

The vertebra geometry is incorporated in the model by establishing the coordinates of the load application points, and of the origins

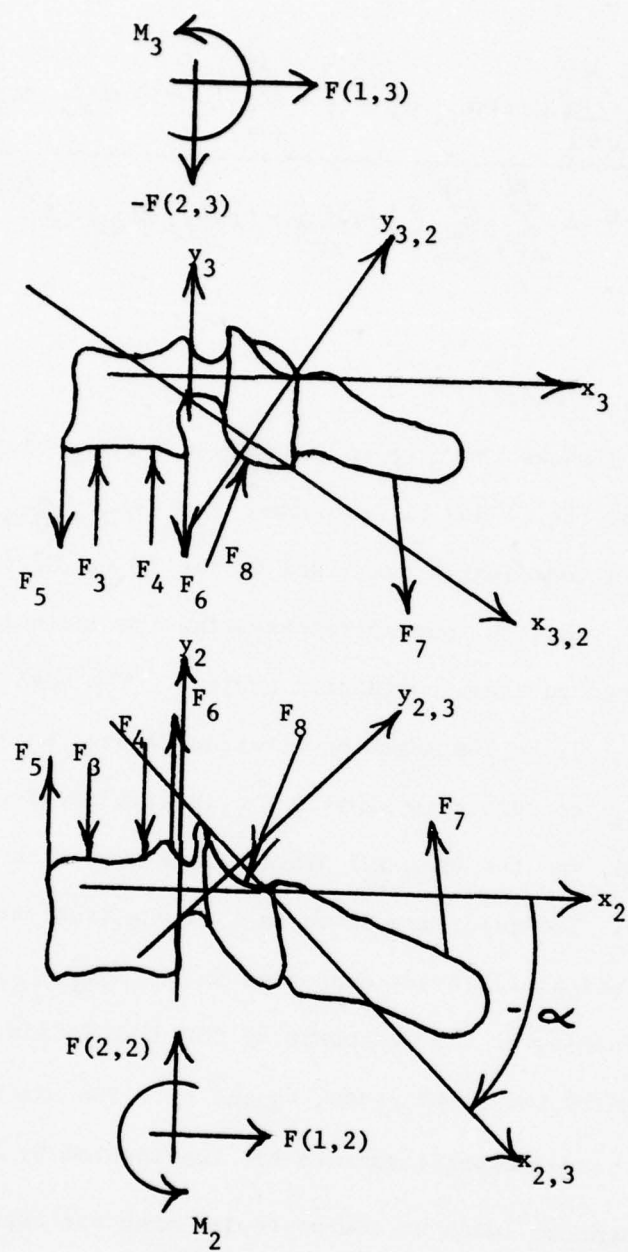


FIGURE 2.3 - FREE BODY DIAGRAM

of the coordinate systems in which the articulating facets are described. For T1, the load point coordinates and the origin of the (x_{23}, y_{23}) system are established in the (x_2, y_2) system, and for C7, the load points coordinates are established in the (x_{32}, y_{32}) system.

If the model were to be expanded to three or more bodies representing two or more vertebral joints, the top and bottom vertebrae would be identical to Fig 2.3. Any intervening vertebrae would have two coordinate systems, fixed to the body, in which the articulating facet curves would be established. The load application points, as well as the origin of the superior coordinate system, would be defined in the inferior system.

The remaining kinematics required are the vector transformation between coordinate systems and the expression for the vector between points of adjacent bodies. The vector transformation is the same as equation 2.3, with appropriate subscripts and angle γ . The expression for the vector between points on adjacent bodies is shown in equation 2.5. Terms of the form $x(i,j)$ and $y(i,j)$

$$\vec{R}_{mm}^{lk} = [-x(l,m) + x(l,2) + x_{lk} \cos \alpha - y_{lk} \sin \alpha + (x(k,n) - x_{kl}) \cos(\alpha + \gamma) - (y(k,n) - y_{kl}) \sin(\alpha + \gamma)] \vec{x}_l + [-y(l,m) + y(l,2) + x_{lk} \sin \alpha + y_{lk} \cos \alpha + (x(k,n) - x_{kl}) \sin(\alpha + \gamma) + (y(k,n) - y_{kl}) \cos(\alpha + \gamma)] \vec{y}$$
(2.5)

where: l - inferior body
 k - superior body
 m - point on inferior body
 n - point on superior body
 α - angle between coordinate systems fixed to the
 inferior body
 δ - angle between coordinate systems fixed to
 adjacent articulating facets.

are the x and y coordinate, respectively, of point "j" on body "i". The x_{ij} and y_{ij} terms are the coordinates of the contact point in the appropriate coordinates fixed to the body. The derivation of equation 2.5 is shown in Appendix A.

2.4 Governing Equations.

Since the mass of the vertebrae is being neglected, the governing equations can be derived from the vectors equations in which the sum of the forces and moments equal zero. These vector equations result in six algebraic equations shown as equations 2.6 through 2.11. The first subscript on the force terms designates the x or y component

$$F_{13} + F_{14} - F_{15} - F_{16} - F_{17} - F_{18} + F(1,2) = 0 \quad (2.6)$$

$$- F_{13} - F_{14} + F_{15} + F_{16} + F_{17} + F_{18} + F(1,3) = 0 \quad (2.7)$$

$$- F_{23} - F_{24} + F_{25} + F_{26} + F_{27} - F_{28} + F(2,2) = 0 \quad (2.8)$$

$$F_{23} + F_{24} - F_{25} - F_{26} - F_{27} + F_{28} + F(2,3) = 0 \quad (2.9)$$

$$\begin{aligned}
 M_2 + \sum_{i=3}^7 [x(1,i)F_{2i} - y(1,i)F_{1i}] &+ (x(1,2) + x_{23} \cos\alpha & (2.10) \\
 - y_{23} \sin\alpha) F_{28} - (y(1,2) + x_{23} \sin\alpha + y_{23} \cos\alpha) F_{18} \\
 = 0
 \end{aligned}$$

$$\begin{aligned}
 M_3 + \sum_{i=3}^7 [(xx_i \cos(\alpha+\delta) - yy_i \sin(\alpha+\delta)) F_{2i} - (xx_i \sin(\alpha+\delta) & (2.11) \\
 + yy_i \cos(\alpha+\delta)) F_{1i}] + (xx_8 \cos(\alpha+\gamma) - yy_8 \sin(\alpha+\delta)) F_{28} \\
 - (xx_8 \sin(\alpha+\gamma) + yy_8 \cos(\alpha+\delta)) F_{18} = 0
 \end{aligned}$$

$$\text{WHERE: } xx_i = x(2,i) - x(2,2)$$

$$yy_i = y(2,i) - y(2,2)$$

$$xx_8 = x_{32} - x(2,2)$$

$$yy_8 = y_{32} - y(2,2)$$

of the force in the inertial coordinate system. A "1" subscript designates the x-component and a "2" subscript designates the y-components. The notation convention for the other terms is the same as used above.

Two more relationships can be derived based on the fact that the direction of the contact force (F_8) is normal to the articulating facet curve; i.e. $F_8 = F_8 \frac{\vec{\nabla} f}{|\vec{\nabla} f|}$. The vector equation yields the two algebraic equations shown as equations 2.12 and 2.13 after they have been transformed to the inertial coordinate system.

$$(2.12) \quad F_{18} = F_8 \frac{\left[\left(\sum_{i=1}^N (i-1) a_{1i} x_{23}^{(i-2)} \right) \cos \alpha + \sin \alpha \right]}{\left[\left(\sum_{i=1}^N (i-1) a_{1i} x_{23}^{(i-2)} \right)^2 + 1 \right]^{1/2}}$$

$$(2.13) \quad F_{28} = F_8 \frac{\left[\left(\sum_{i=1}^N (i-1) a_{1i} x_{23}^{(i-2)} \right) \sin \alpha - \cos \alpha \right]}{\left[\left(\sum_{i=1}^N (i-1) a_{1i} x_{23}^{(i-2)} \right)^2 + 1 \right]^{1/2}}$$

Equations 2.6 through 2.13 along with the constraint equation 2.4, the two functions defining the articulating facet curves (f_1 and f_2), ten component force equations (using equation 2.1) and ten component displacement equations (using equation 2.5) constitute a series of thirty-one simultaneous, nonlinear, algebraic equations. There are also thirty-one variables, which are listed in Table 2.1; therefore, the above set of equations is sufficient to determine the response of the joint model at a given point in time.

Table 2.1

List of Variables x_{23}, y_{23} x_{32}, y_{32} $F(1,2), F(2,2)$ M_2 γ F_8 $d_{ij} \ (i = 1,2; j = 3, 4, 5, 6, 7)*$ $F_{ij} \ (i = 1,2; j = 3, 4, 5, 6, 7, 8)$

* d_{ij} 's are the displacement using equation 2.5.

2.5 Linearization and Solution of Equations.

The set of equations derived above is not only large, but also nonlinear and therefore difficult to solve. The first simplifi-

cation comes from the assumption that γ is small, and hence, 20
 the small angle approximation can be used; i.e., $\sin \gamma = \gamma$,
 $\cos \gamma = 1$ and $\tan \gamma = \gamma$. This assumption is supported
 by data reported by Bhalla and Simmons (1969), in which they
 show the maximum rotation, in the sagittal plane, of the C7 and
 T1 vertebrae to be less than 10 degrees. The small angle approximation
 eliminates the nonlinearity resulting from the trigometric functions.

Following this simplification, Newton's method is applied
 to the equations. Each variable is replaced by an initial guess
 of the variable value plus an error; for example, x_{23} is replaced
 by $x_{23} + \Delta x_{23}$. If the assumption is made that Δx_{23} is small,
 and all the other Δ variables are small, then all second and
 higher order delta terms can be neglected. The equations can
 then be rewritten to solve for the delta variables. The force
 equations can be written:

(2.14)

$$\begin{aligned}\Delta F_{ij} - & [b_{2j} + b_{5j}(\dot{d}_{ij}) + 2b_{3j}(d_{ij}) + 3b_{4j}(d_{ij}^2)]\Delta d_{ij} \\ = & -F_{ij} + b_{1j} + (b_{2j} + b_{5j}(\dot{d}_{ij}))d_{ij} \\ & + b_{3j}(d_{ij}^2) + b_{4j}(d_{ij}^3)\end{aligned}$$

where: $i = 1, 2$

$j = 3, 4, 5, 6, 7$

The functions defining the curves representing the articulating facets become:

21

$$\left(\sum_{j=2}^N (j-1) a_{ij} x^{(j-2)} \right) \Delta x - \Delta y = \\ - \left(\sum_{j=1}^N a_{ij} x^{(j-1)} \right) + y \quad (2.15)$$

where: $x = x_{23}$ or x_{32} and

$y = y_{23}$ or y_{23} respectively

$i = 1, 2$

The constraint equation becomes:

$$(1 + s_1) \Delta x + y (s_2) - (s_3 - s_4) = \\ -y(1 + s_1) - \sum_{i=1}^N (i-1) a_{1i} x_{23}^{(i-2)} + \sum_{j=1}^M (j-1) a_{2j} x_{32}^{(j-2)} \quad (2.16)$$

where: $s_1 = \sum_{i=1}^N \sum_{j=1}^M (i-1)(j-1) a_{1i} a_{2j} x_{23}^{(i-2)} x_{32}^{(j-2)}$

$$s_2 = \sum_{i=1}^N \sum_{j=1}^M (i-1)(j-1) a_{1i} a_{2j} \left((j-2) x_{32}^{(j-2)} \Delta x_{23} \right. \\ \left. + (i-2) x_{23}^{(i-2)} \Delta x_{32} \right)$$

$$S_3 = \sum_{i=1}^N (i-1)(i-2) a_{1,i} \Delta x_{23}$$

$$S_4 = \sum_{j=1}^M (j-1)(j-2) a_{2,j} \Delta x_{32}$$

The resulting x-displacements are shown by equation 2.17, and the resulting y-displacements are equation 2.18.

(2.17)

$$\begin{aligned} \Delta d_{1,i} - (\cos \alpha) \Delta x_{23} + (\sin \alpha) \Delta y_{23} + Q(2) \Delta x_{32} \\ - Q(1) \Delta y_{32} + [(x_{(2,i)} - x_{32}) \sin \alpha + \\ (y_{(2,i)} - y_{32}) \cos \alpha] \Delta \gamma = (\cos \alpha) x_{23} \\ - (\sin \alpha) y_{23} - (x_{32} - x_{(2,i)}) Q(2) \\ - (y_{32} - y_{(2,i)}) Q(1) - x_{(1,i)} + x_{(1,2)} \\ - I_{1,i} - d_{1,i} \end{aligned}$$

(2.18)

$$\begin{aligned}
 \Delta d_{2i} - (\sin \alpha) \Delta x_{23} - (\cos \alpha) \Delta y_{23} + Q(1) \Delta x_{32} \\
 Q(2) y_{32} + [(x(2,i) + x_{32}) \cos \alpha + (y(2,i) - y_{32}) \sin \alpha] \Delta \gamma = \\
 (\sin \alpha) x_{23} + (\cos \alpha) y_{23} - (x_{32} - x(2,i)) Q(1) \\
 - (y_{32} + y(2,i)) Q(2) - y(1,i) + y(1,2) \\
 - I_{2i} - d_{2i}
 \end{aligned}$$

where: d_{1i} = x displacement

d_{2i} = y displacement

$Q(1) = \sin \alpha + \gamma \cos \alpha$

$Q(2) = \cos \alpha - \gamma \sin \alpha$

$i = 3, 4, 5, 6, 7$

The equations for the x and y components of normal contact force on the facets are equations 2.19 and 2.20 respectively.

(2.19)

$$\begin{aligned}
 & \left[F_{18}^2 (55) - F_8^2 ((55) \cos^2 \alpha + 2 (57) \cos \alpha \sin \alpha) \right] \\
 & + 2 F_{18} ((56) + 1) \Delta F_{18} - 2 F_8 ((56) \cos^2 \alpha + \\
 & 2 (58) \cos \alpha \sin \alpha + \sin^2 \alpha) \Delta F_8 = F_{18}^2 ((56) + 1) \\
 & + F_8^2 ((56) \cos^2 \alpha + 2 (58) \cos \alpha \sin \alpha + \sin^2 \alpha)
 \end{aligned}$$

(2.20)

$$\begin{aligned}
 & \left[F_{28}^2 (S5) - F_8^2 ((S5) \sin^2 \alpha - 2(S7) \cos \alpha \sin \alpha \right. \\
 & + 2F_{28}((S6)+1) \Delta F_{28} - 2F_8 ((S6) \sin^2 \alpha - \\
 & \left. 2(S8) \cos \alpha \sin \alpha + \cos^2 \alpha \right) \Delta F_8 = \\
 & - F_{28}^2 ((S6+1) + F_8^2 ((S6) \sin^2 \alpha - \\
 & 2(S8) \cos \alpha \sin \alpha + \cos^2 \alpha)
 \end{aligned}$$

WHERE :

$$S(5) = \sum_{i=1}^N \sum_{j=1}^N (i-1)(j-1) a_{1i} a_{1j} (i-2)(j-2) \\
 (x^{(i+j-5)} \Delta x_{23})$$

$$S(6) = \sum_{i=1}^N \sum_{j=1}^N (i-1)(j-1) a_{1i} a_{1j} x_{23}^{(i+j-4)}$$

$$S(7) = \sum_{i=1}^N (i-1) a_{1i} (i-2) x_{23}^{(i-3)} \Delta x_{23}$$

$$S(8) = \sum_{i=1}^N (i-1) a_{1i} x_{23}^{(i-2)}$$

The remaining 6 equations are those derived from the sum of the forces and moments on each body. Equations 2.21, 22, and 23 relate to body 2 and equations 2.24, 25, and 26 relate to body 3.

(2.21)

$$\Delta F(1,2) + \Delta F_{1,3} + \Delta F_{1,4} - \Delta F_{1,5} - \Delta F_{1,6} - \Delta F_{1,7} - \Delta F_{1,8} = \\ - [F(1,2) + F_{1,3} + F_{1,4} - F_{1,5} - F_{1,6} - F_{1,7} - F_{1,8}]$$

(2.22)

$$\Delta F(2,2) - \Delta F_{2,3} - \Delta F_{2,4} + \Delta F_{2,5} + \Delta F_{2,6} + \Delta F_{2,7} - \Delta F_{2,8} = \\ - [F(2,2) - F_{2,3} - F_{2,4} + F_{2,5} + F_{2,6} + F_{2,7} - F_{2,8}]$$

(2.23)

$$\sum_{j=3}^4 (\Delta F_{1,j} y(1,j) + \Delta F_{2,j} x(1,j)) - \sum_{j=5}^7 (\Delta F_{1,j} y(1,j) \\ + \Delta F_{2,j} x(1,j)) - (y(1,2) + x_{2,3} \sin \alpha + y_{2,3} \cos \alpha) \Delta F_{1,8} \\ + (x(1,2) + x_{2,3} \cos \alpha - y_{2,3} \sin \alpha) \Delta F_{2,8} \\ - (F_{1,8} \sin \alpha - F_{2,8} \cos \alpha) \Delta x_{2,3} - (F_{1,8} \cos \alpha + F_{2,8} \sin \alpha) \Delta y_{2,3} \\ - \Delta M_2 = - \sum_{j=3}^4 (F_{1,j} y(1,j) + F_{2,j} x(1,j)) \\ + \sum_{j=5}^7 (F_{1,j} y(1,j) + F_{2,j} x(1,j)) + (y(1,2) + x_{2,3} \sin \alpha \\ + y_{2,3} \cos \alpha) F_{1,8} - (x(1,2) + x_{2,3} \cos \alpha - y_{2,3} \sin \alpha) F_{2,8}$$

$$-\Delta F_{13} - \Delta F_{14} + \Delta F_{15} + \Delta F_{16} + \Delta F_{17} + \Delta F_{18} = \quad (2.24)$$

$$-F(1,3) - [-F_{13} - F_{14} + F_{15} + F_{16} + F_{17} + F_{18}]$$

$$\Delta F_{23} + \Delta F_{24} - \Delta F_{25} - \Delta F_{26} - \Delta F_{27} + \Delta F_{28} = \quad (2.25)$$

$$-F(2,3) - [F_{23} + F_{24} - F_{25} - F_{26} - F_{27} + F_{28}]$$

$$\sum_{j=3}^4 (S9_j \Delta F_{1j} + S10_j \Delta F_{2j}) - \sum_{j=5}^7 (S9_j \Delta F_{1j} + S10_j \Delta F_{2j}) \quad (2.26)$$

$$-(xx_g Q(1) + yy_g Q(2)) \Delta F_{18} + (xx_g Q(2) - yy_g Q(1)) \Delta F_{28}$$

$$+ (Q(2) F_{28} - Q(1) F_{18}) \Delta \gamma_{32} - (Q(1) F_{28} + Q(2) F_{18}) \Delta \gamma_{32}$$

$$- \left[\sum_{j=3}^4 S11_j - \sum_{j=5}^7 S11_j - (xx_g \sin \alpha - yy_g \cos \alpha) F_{28} \right.$$

$$\left. + (xx_g \cos \alpha - yy_g \sin \alpha) F_{18} \right] \Delta \gamma =$$

$$- \left[M_3 + \sum_{j=3}^4 (S10_j F_{2j} + S9_j F_{1j}) - \sum_{j=5}^7 (S10_j F_{2j} + \right.$$

$$\left. S9_j F_{1j}) + (xx_g Q(2) - yy_g Q(1)) F_{28} - \right.$$

$$(xx_g Q(1) + yy_g Q(2)) F_{18}$$

Where:

$$S9_j = (C_{2j} + \gamma C_{1j})$$

$$S10_j = (C_{1j} - \gamma C_{2j})$$

$$S11_j = (C_{2j} F_{2j} - C_{1j} F_{1j})$$

$$C_{1j} = (xx_j \cos\alpha - yy_j \sin\alpha)$$

$$C_{2j} = (xx_j \sin\alpha + yy_j \cos\alpha)$$

$$xx_j = x(z_j) - x(z_z)$$

$$yy_j = y(z_j) - y(z_z)$$

$$xx_8 = x_{3z} - x(z_z)$$

$$yy_8 = y_{3z} - y(z_z)$$

$$Q(1) = \sin\alpha + \gamma \cos\alpha$$

$$Q(2) = \cos\alpha - \gamma \sin\alpha$$

If the 31 equations generated from equations 2.14 through 2.25 are put into matrix format, Gaussian elimination with pivotal condensation and back substitution can be used to solve for the delta variable values. The initial guess at the variable is adjusted by the delta value and the process is iterated until the delta

value becomes small. When the series of iterations is completed, the input values are incremented for the next time interval and the whole process is repeated for as many time intervals as desired. The initial guess can be obtained by solving the static problem at time equal to zero, and the solution for the last time interval is used as the initial guess for the following iterations.

A listing of the computer program to carry out the iterative solution is included at the end of this dissertation.

CHAPTER III

EXPERIMENTAL CHARACTERIZATION OF LIGAMENT MATERIAL PROPERTIES

3.1 Background.

As stated in Chapter I, there are very limited data published which describe the mechanical response of the human spinal ligaments, and the data that are available deal only with the lumbar regions of the spine. Akerblom (1948) ran some experiments in which he removed the posterior arches from a series of lumbar vertebrae such that the arches and spinous processes were attached only by the interspinal and supraspinal ligaments. The series of arches was then suspended and loaded with a series of weight up to 40 kg and the resultant deflections recorded. He concluded that the ligaments are nonlinearly elastic up to 20 kg of load; however there is no time information recorded, so in essence, what is reported are the end points for a series of creep tests. In addition, no dimensional information on the test specimens is reported and therefore this data was of no use in the present effort. Nachemson and Evans (1968) conducted experiments again using the ligaments of the posterior column between the third and fourth lumbar vertebrae. They report a nominal stress vs. strain plot which is of similar shape to the data I generated. Two problems exist with these data: the lack of any dimensional data on the test specimens and the ambiguity in the strain rate used, which is reported to be "+0.33 min." and "0.33/min." Either the authors neglected to report units or the 0.33 min. was the time period during which the load cycle was applied in

which case the claim of a constant strain rate is erroneous.

30

The best data found in the literature were reported by Tkaczuk (1968) concerning his investigation of the tensile properties of the anterior and posterior longitudinal ligaments of the human lumbar spine.

He conducted tensile tests with both intact ligaments and identical test specimens cut from the whole ligament with a cross sectional area of 1 mm^2 . He reports test specimen dimensions, yield and failure loads, as well as load vs deflection data for tests run at a constant loading rate in which the specimen was cycled from 0 to 500 gm in 35 sec. His curves are similar in shape to my results and a comparison will be made later in this chapter.

3.2 Experimental Approach.

Because of the very limited data on spinal ligament response properties, an experimental effort was conducted to generate some experimental results on test specimens taken from the C6-C7-T1 region of the spine. Only the anterior longitudinal ligament (A.L.L.) and the posterior longitudinal ligament (P.L.L.) were tested.

The initial approach was to conduct relaxation tests with the hope that a relaxation modulus could be established. With these data, linear viscoelasticity theory such as presented by Flugge (1967) could be used to characterize the ligament dynamic response. Three specimens (C6-C7 A.L.L.; C6-C7 P.L.L.; C7-T1 A.L.L.) were used in a series of nine relaxation tests; the results of which were totally confusing. The load vs. time plots were typical for a viscoelastic material, however there was no correlation in the data for a given specimen tested at different magnitudes

of deflection or for different specimens tested identically.

At the time, the reasons for the confusing results were not obvious, and it appeared that to continue with this approach, a much more extensive test series requiring a large number of test specimens would be necessary. The required number of test specimens was not available and it was decided that such an extensive characterization of ligament material properties was beyond the scope of this effort. Hence an alternative approach was taken.

Since most neck injuries occur during accidents where the loading is applied over a time interval lasting only 100 to 200 millisec., it was decided to conduct tensile tests using relatively high loading rates. In doing so, the resulting data are restricted to this loading regime, and any model in which it is used is likewise restricted. With this approach, it was hoped that the response of the ligament, both during loading and unloading, could be characterized, and that the effect of the loading rate, if any, on the response could be determined.

From X-rays of the author's neck, the deformation of the anterior and posterior longitudinal ligaments during normal motion was determined to range up to 0.1 in. From this fact, and using the 100 to 200 millisec. time interval, which was determined from a perusal of reports dealing with human volunteer tests, the loading rates were chosen. Referring to Fig 3.1, the load was applied in a triangular pulse where Δe varied from 0.03 in. to 0.10 in., and Δt was set to give the desired loading rate.

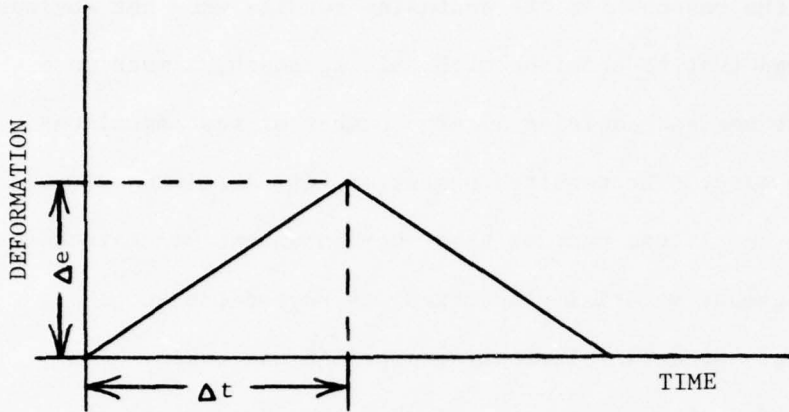


FIGURE 3.1 - SHAPE OF LOADING PULSE

The following procedures were followed throughout the testing program. The night before a test, the spinal segment, from which the specimen would be removed, was moved from the storage freezer to a refrigerator to thaw out. In the morning, the segment was X-rayed and the specimen was prepared as described in Section 3.3 below, and loaded in the test fixture which is described in Section 3.4. The fixture and specimen were then wrapped in moist gauze and sealed in a plastic bag to prevent dehydration of the specimen. Following the above procedures, which were conducted at the Aerospace Medical Research Laboratory, WPAFB, the test fixture was then taken to the University of Dayton Research Institute, where the actual tests were conducted.

In the following sections of this chapter is a description of the specimen preparation, the test fixture used to hold the specimens and finally a detailed description of the test parameters and results.

3.3 Test Specimen Preparation.

After the thawed spinal segments had been X-rayed (Figures 3.2, 3.3, 3.4 and 3.5), the posterior arches were removed by cutting through the pedicles of each vertebrae with a band saw, as shown in Fig 3.6, cuts 1 and 2. After extraneous material was removed from the top and bottom of the segment, a lateral cut was made through the vertebrae bodies shown in Fig 3.6 as cut 3. Following this cut, the intervertebral disc and any other remaining soft tissue was surgically removed using care not to cut either of the longitudinal ligaments. This procedure produced

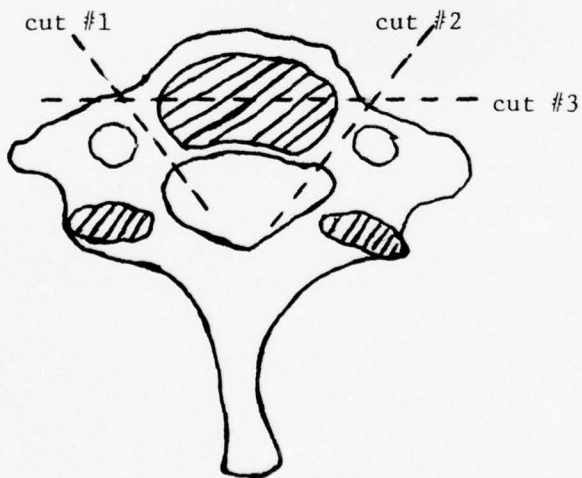


FIGURE 3.2 - SPECIMEN PREPARATION - SAW CUTS



FIGURE 3.3 - X-RAY -- SPECIMEN 11X AND 12X

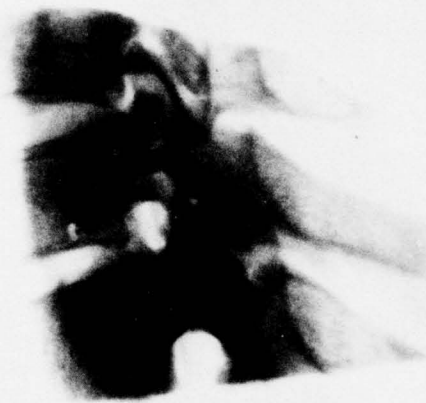


FIGURE 3.4 - X-RAY -- SPECIMEN 13X AND 14X



FIGURE 3,5 - X-RAY -- SPECIMEN 15X AND 17X



FIGURE 3.6 - X-RAY -- SPECIMEN 18X, 19X, 20X AND 21X

two specimens consisting of either the anterior or posterior sections of two adjacent vertebral bodies connected by the anterior or posterior longitudinal ligament respectively. Fig. 3.7 shows both an anterior and posterior specimen prior to having the intervertebral disc removed.

3.4 Test Fixture and Equipment.

The test fixture developed and used for these tests consisted of two aluminum blocks milled to have a lip along one side; parallel to each lip was attached a semi-circular bridge which was drilled and tapped for four screws at various angles. A sketch of a single block is shown in Fig. 3.8. The two blocks were positioned such that the sides with the lips were butted together and the blocks were held in position during handling with straps bolted

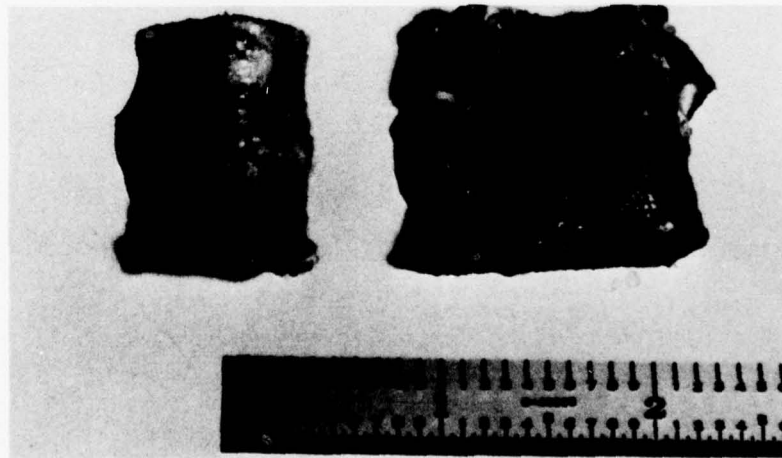


FIGURE 3.7 - TEST SPECIMEN PRIOR TO REMOVAL OF DISC

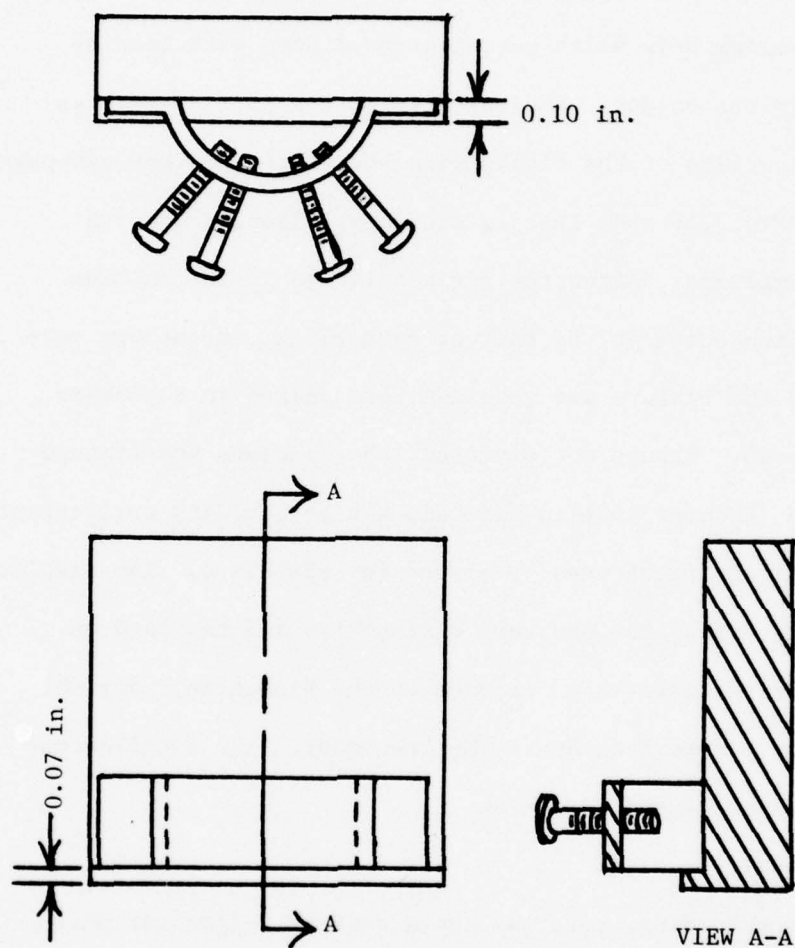


FIGURE 3.8 - TEST FIXTURE

along the sides. The ligament specimen was positioned in the jig with the flat sides of the vertebral bodies against the block and under the bridge with the lips protruding between the two body segments. The specimen was then clamped between the blocks and four aluminum pads which were tightened down with four of the screws in the bridge. The surfaces of the pads as well as the contact surface of the blocks were knurled to prevent slippage.

Fig. 3.9 and Fig. 3.10 show the jig with a specimen, loaded in the tensile machine. After the jig was loaded in the machine by means of two bolts in the back of each block, the straps were loosened and the fixture and specimen were sealed in a plastic sleeve as shown. Though not pictured, the specimen and fixture were wrapped in damp gauze to maintain a high humidity environment.

The test equipment used is listed in Appendix A. The displacement vs. time data during the pre-test calibration and the load vs. time data during tests were recorded on the Biomation Transient Recorder then played back on the X-Y recorder. The oscilloscope was used as a back-up data system.

3.5 Test Results.

The true loading rate was not a perfect triangular pulse as shown in Fig. 3.1 due to limitations of the MTS machine used; however, previous to each day's testing the machine was calibrated and deformation vs. time curves were recorded. The top of the triangular pulse tended to be rounded off. Table 3.1 provides the identification and the dimensional data for each specimen, and Appendix B lists the parameters for each test.

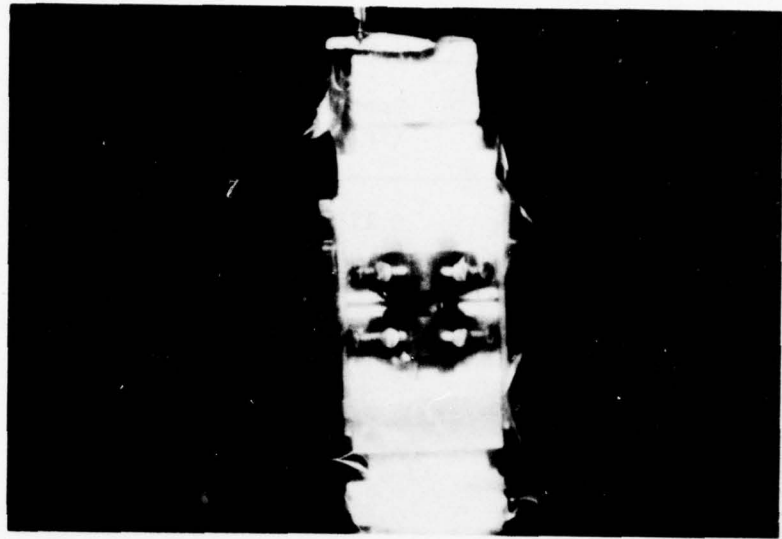


FIGURE 3.9 - SPECIMEN LOADED IN FIXTURE

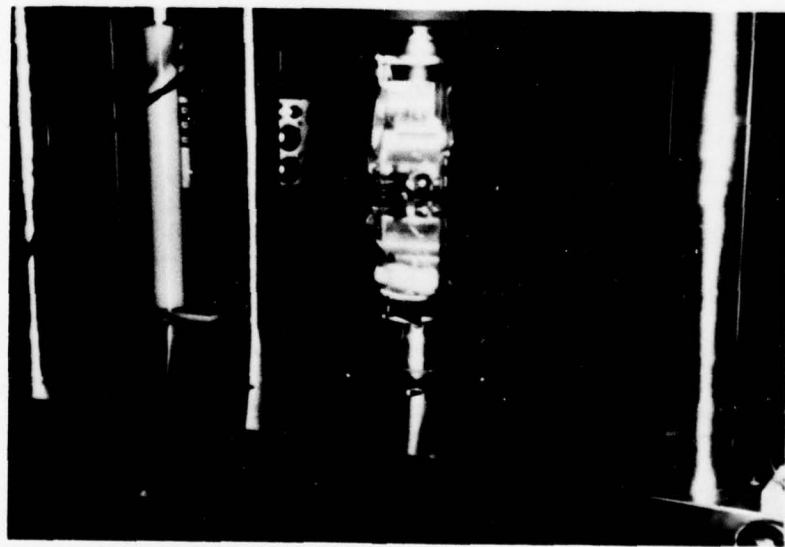


FIGURE 3.10 - FIXTURE IN TENSILE TEST MACHINE

Table 3.1

Specimen Identification and Dimensions

Specimen Number	Ligament	Width* (in.)	Depth* (in.)	Length** (in.)	Intervertebral Height at Cut (in.)***
11X	C6-C7, A.L.L.	0.669	0.110	0.27	0.14
12X	C6-C7, P.L.L.	0.384	0.149	0.26	0.14
13X	C7-T1, A.L.L.	0.638	0.089	0.24	0.17
14X	C7-T1, P.L.L.	0.409	0.095	0.21	0.17
15X	C7-T1, A.L.L.	0.402	0.059	0.23	0.18
17X	C7-T1, P.L.L.	0.337	0.087	0.22	0.18
18X	C6-C7, A.L.L.	0.551	0.067	0.31	0.23
19X	C7-T1, A.L.L.	0.630	0.055	0.26	0.14
20X	C6-C7, P.L.L.	0.260	0.055	0.24	0.23
21X	C7-T1, P.L.L.	0.366	0.057	0.21	0.14

* Measurements were made with a caliper at the time of specimen preparation, and since the tissue being measured is soft, the resulting measurements are subject to some variation in measurement technique.

** Measurements were made on X-rays of specimens taken prior to specimen preparation, and are nominal lengths measured between the prominent margins of the vertebrae.

*** Measurements are taken from X-rays at the point where the lateral cut was made during specimen preparation.

As stated in 3.2 above, the deflection of the longitudinal ligaments during normal motion was determined to be approximately 0.10 in., and this was used as the maximum deflection during

the early tests. It was discovered after the first several tests that yielding was occurring well below the 0.10 in. extension. In fact, yielding occurred at extensions between 0.50 and 0.70 in. In the 15X specimen the initial extension was 0.50 in., and in all following tests the initial extensions were 0.30 in. Therefore, data from specimens 11X through 14X are not used except in comparing yield loads and stresses with those of Tkaczuk (1968). However it should be noted that tests conducted after yielding occurred, and at maximum extensions equal to or less than those in which yielding occurred, gave very repeatable results.

Another phenomenon was also discovered during the analysis of the test data, and for illustration, Fig. 3.11 through 3.16 show load vs. deflection curves for tests using specimen 17X. Fig. 3.11 shows good repeatability between two identical tests which were conducted at the higher deflection rate of 1.0 in./sec. Fig. 3.12 shows a comparison between tests at two different loading rates which result in different shape curves. The lower extension rate of 0.5 in./sec. appears to have less hysteresis in its response, as well as a lower magnitude during the positive loading portion of the load cycle. The curve at the lower loading rate is also repeatable as shown in Fig. 3.13. However in the following test, number 175 which was at the higher rate, the loading curve follows the loading curve of the previous test which was at the 0.5 in./sec. rate. See Fig. 3.14. Similar response is seen again in the following tests shown in Fig. 3.15 and 3.16. It is concluded that some permanent damage must have occurred during the lower loading rate tests from which the specimen did not recover, and there

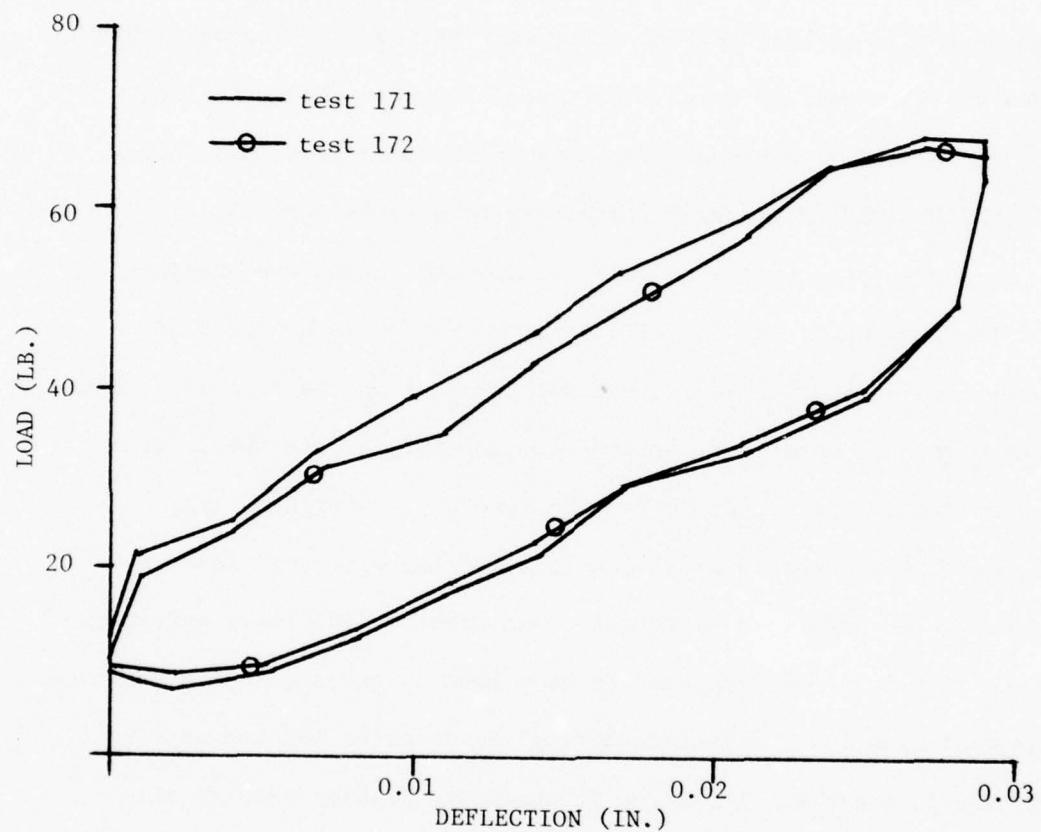


FIGURE 3.11 - LOAD VS. DEFLECTION

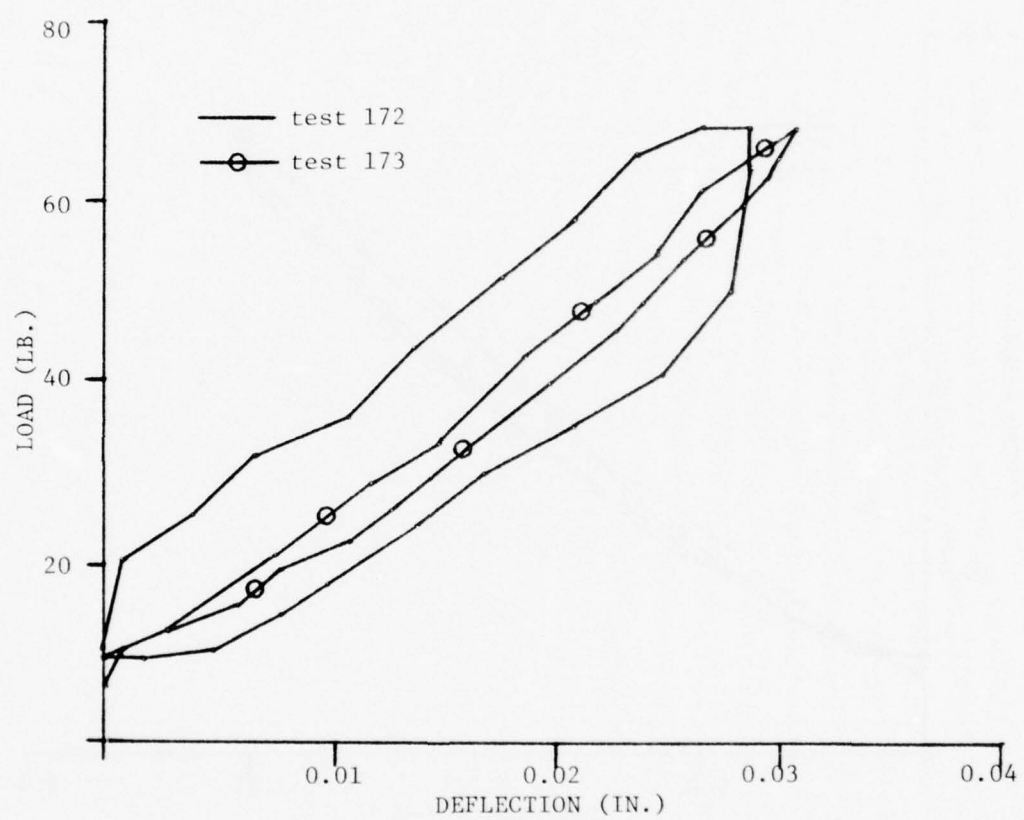


FIGURE 3.12 - LOAD VS. DEFLECTION

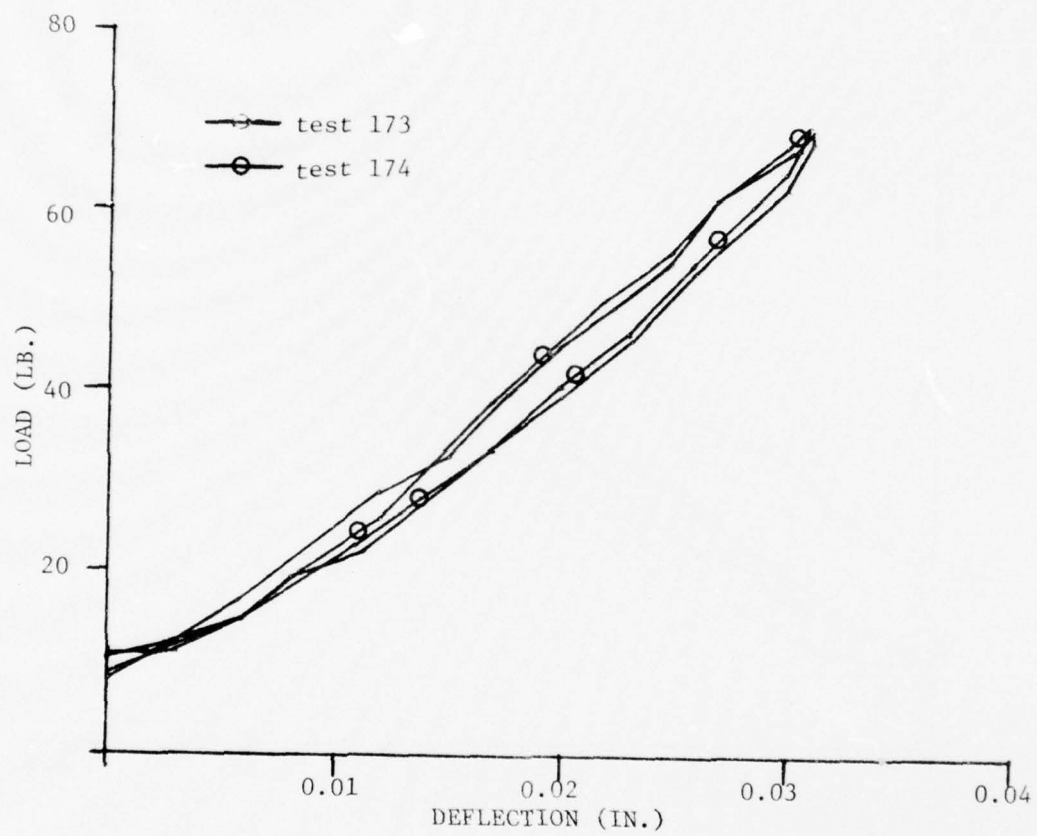


FIGURE 3.13 - LOAD VS. DEFLECTION

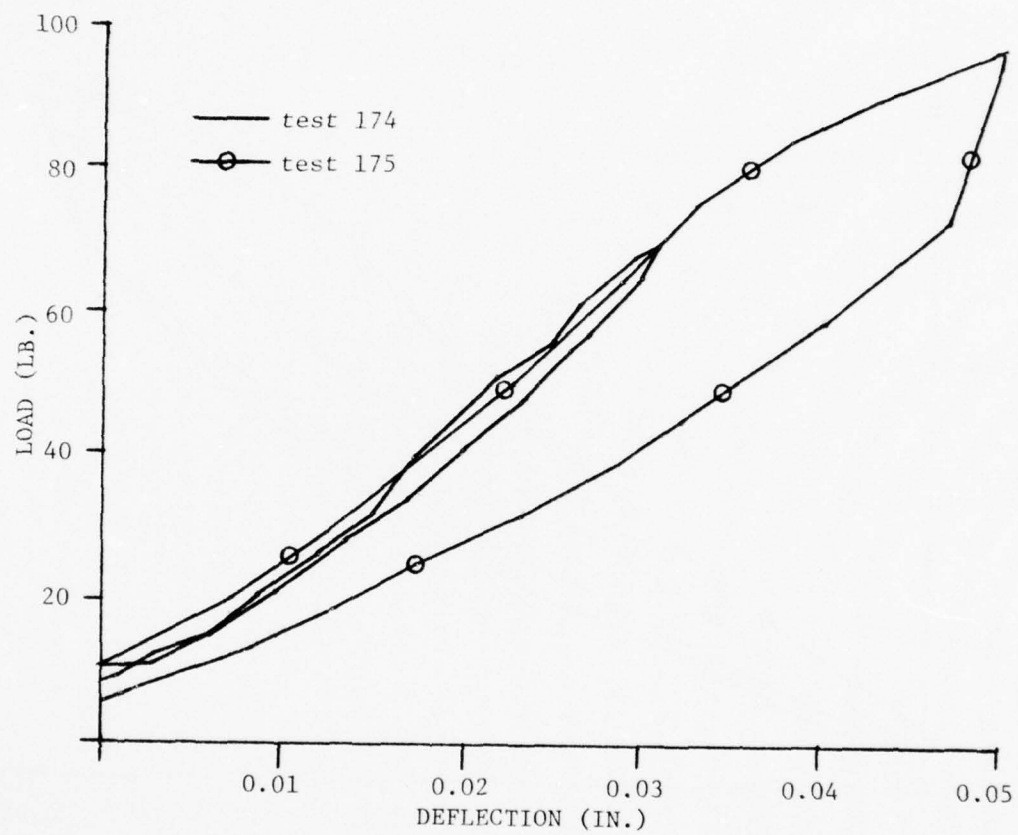


FIGURE 3.14 - LOAD VS. DEFLECTION

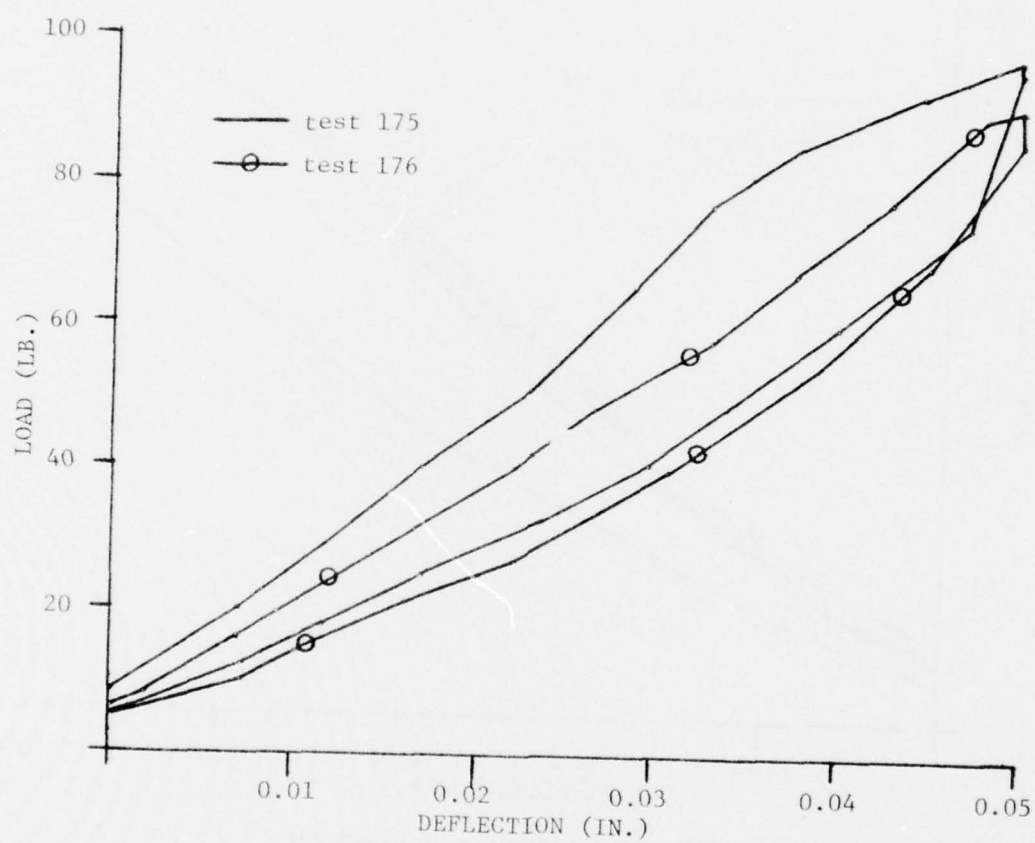


FIGURE 3.15 - LOAD VS. DEFLECTION

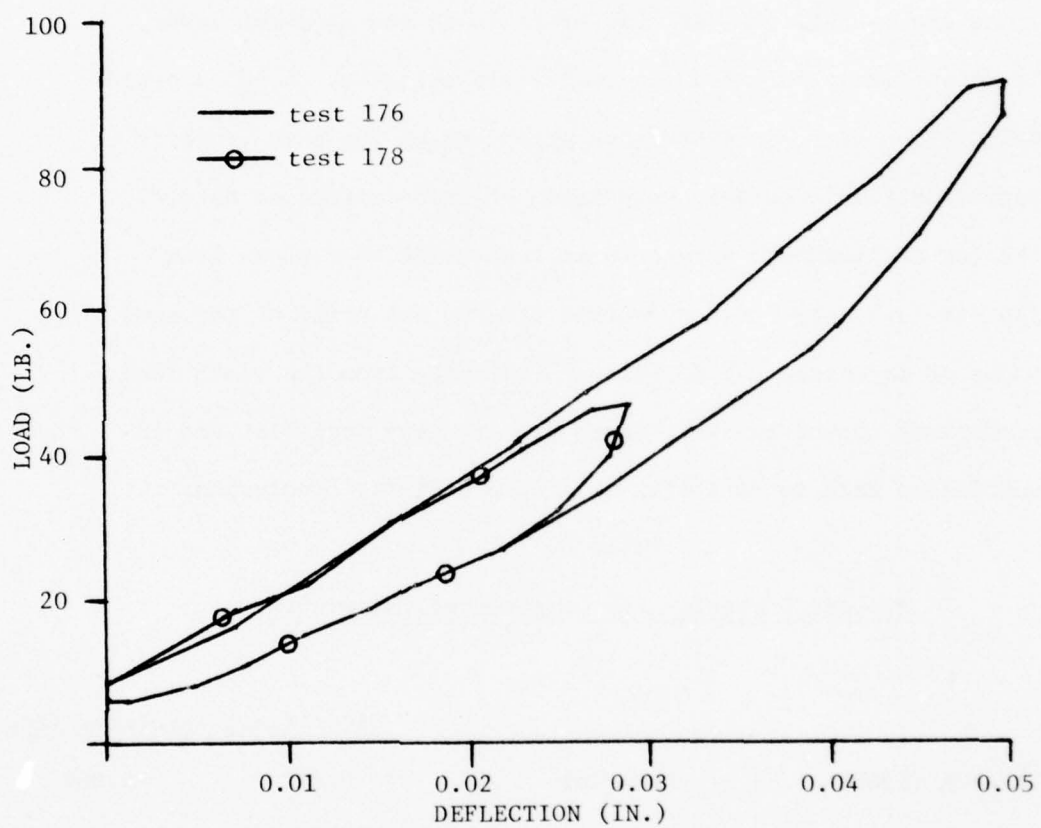


FIGURE 3.16 - LOAD VS. DEFLECTION

was a gradual degredation in the specimen during a series of tests as can be seen by comparing Fig. 3.11 and 3.16. This sequence of response was typical during all tests in the latter portion of the test program.

Tables 3.2, 3.3 and 3.5 show a brief comparison between data generated in this effort and those of Tkaczuk (1968). As would be expected, the ligaments Tkaczuk used from the lumbar spine are larger, however, his yield loads are somewhat lower. It is difficult to calculate real yield stresses, though a crude calculation does yield stresses which are of the same order of magnitude. In a cursory comparison of load-deflection data, the lumbar ligaments appear to be less stiff than those from the cervical spine tested in this effort, but still of the same order of magnitude. This follows logically from the yield load comparison above; however, there are too many variables and insufficient data to establish this as a definite conclusion.

Table 3.2
Average Dimension for Longitudinal Ligaments

		Width (in.)	Thickness (in.)
Tkaczuk (1968)	Anterior	0.892	0.064
	Posterior	0.525	0.047
Current Effort	Anterior	0.528	0.060
	Posterior	0.321	0.066

Table 3.3

Ligament Yield Loads

<u>Test Number</u>	<u>Ligament</u>	<u>Yield Load (lb)</u>
111	A.L.L.	112
121	P.L.L.	98
132	A.L.L.	168
141	P.L.L.	95
179	P.L.L.	96
187	A.L.L.	134
204	P.L.L.	86
217	P.L.L.	98
<hr/>		
Average	A.L.L.	138
Average	P.L.L.	94.6
<hr/>		

Table 3.4

Comparison of Average Yield Loads

	<u>Yield Loads (lb)</u>	
	<u>A.L.L.</u>	<u>P.L.L.</u>
Tkaczuk (1968)	57.3	36.2
Current Effort	138	94.6

In concluding this chapter, two observations should be made. First, the longitudinal ligaments in vivo are long, continuous

bands of fibrous material. This condition was not maintained during this effort, in that the ligament was severed on both ends of the specimen. Prior to testing the ligament, bundles appeared tightly packed and allowed very limited lateral or anterior-posterior motion between the two vertebrae body segments. In contrast, after tests had been completed on a specimen, the ligament was looser, appeared to be thinner, and considerably more motion was possible between the body segments. This observation is not surprising in that yielding had occurred and hence the ligament should appear stretched. However, the possibility also exists that there is failure in the adhesion between fibers within the ligament bundle particularly at the primary attachment points on the vertebrae bodies. Prior to any future tests, this problem should be investigated and a possible alternative to severing the ligament considered. The second observation that should be made was on specimen 11X. Following testing of this specimen and removal from the jig, a failure was discovered and is shown in Fig. 3.17 and 3.18. The ligament was severed at approximately the center of one vertebra body and the attachment to the bone was sheared between the point of failure and the margin. It was impossible to determine which failure occurred first, and it was the only time during the testing that such a failure was observed. Since the deflection in test 118 was 0.15 in., which was the only time this large a deflection was used, it is concluded that the failure occurred during the final test on this ligament. The oscilloscope trace shows the load to peak prior to the maximum deflection; however, there is no sudden

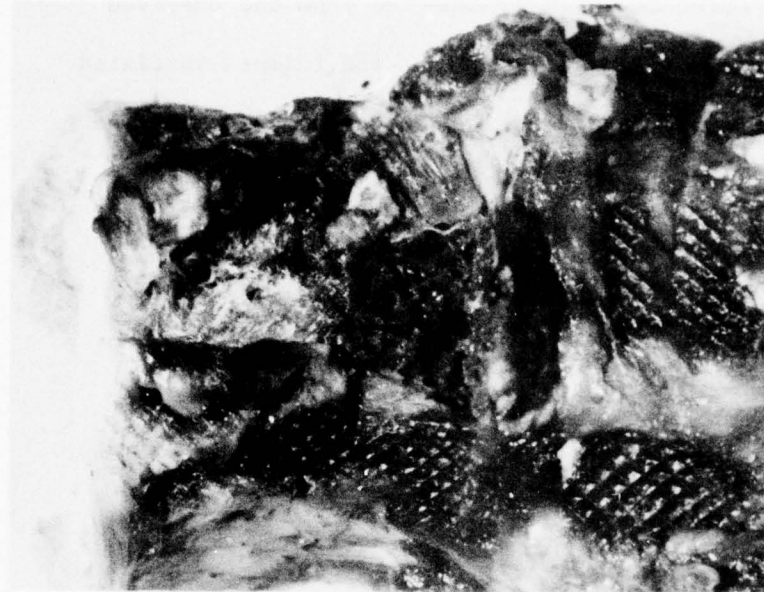


FIGURE 3.18 - FAILURE IN SPECIMEN 11x

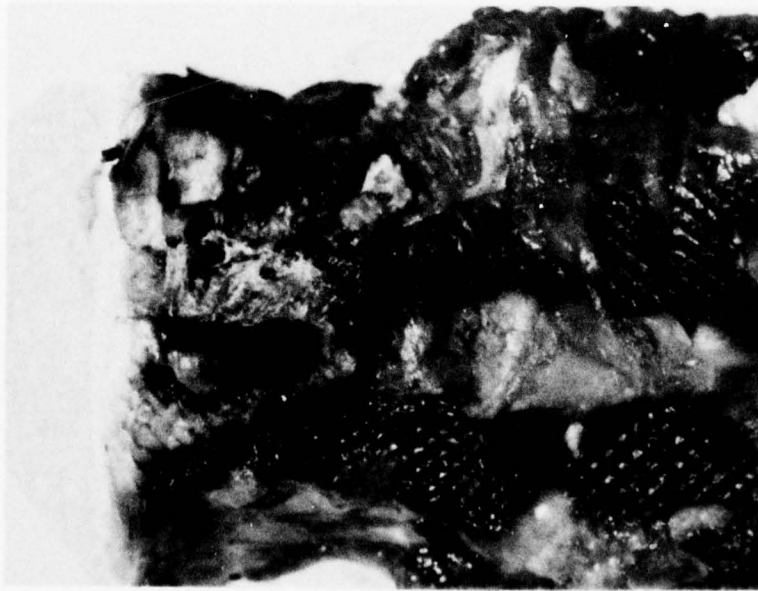


FIGURE 3.17 - FAILURE IN SPECIMEN 11x

drop in the load curve as would be expected from the observed failure. Therefore, it is concluded that the failure initiated at an extension of 0.13 to 0.14 in. and occurred over a period of 10 to 15 millisec.

CHAPTER IV

CONSTITUTIVE EQUATIONS

4.1 Anterior and Posterior Longitudinal Ligament Response.

Following the experimental effort discussed in Chapter III, the next effort was to express the ligament response by some function. The first approach was to use a hereditary integral, as is used in classical viscoelasticity, with an assumed series of exponentials for the relaxation modulus. This approach presupposes that the material is linearly viscoelastic, which was not believed to be true. Therefore, a third order polynomial was superimposed on the hereditary integral, to at least account for nonlinearities in the response as a function of deflection. A least squares curve fit, as discussed by Homming and Feigenbaum (1971) and McCracken and Dorn (1964), was then applied to each set of test data to determine the values for the arbitrary constants in the response function.

The functions were then plotted and compared to the test data. The representation of the response in a given test by the function whose constants had been derived from fitting that particular set of data was excellent; however, difficulty arose in choosing a representative set of constants. There was no obvious trend in the constants even when test data from different tests on the same specimen were used.

As a result of this difficulty, the function expressed in Chapter II as equation 2.1 was investigated. The third order polynomial would account for the nonlinear response, dependent on the magnitude of the deflection, and the (\dot{xx}) term provided a velocity dependence, which is characteristic of viscoelastic materials.

If the displacement was a perfect triangular pulse as shown in Fig. 3.1, the response of the function would be as shown in Fig. 4.1.

If the apex of the loading pulse is rounded off, as was the case during the experimental work, the points of the response curve would also be rounded as shown by the dotted lines in Fig. 4.1. This shape curve showed potential for representing the experimental results.

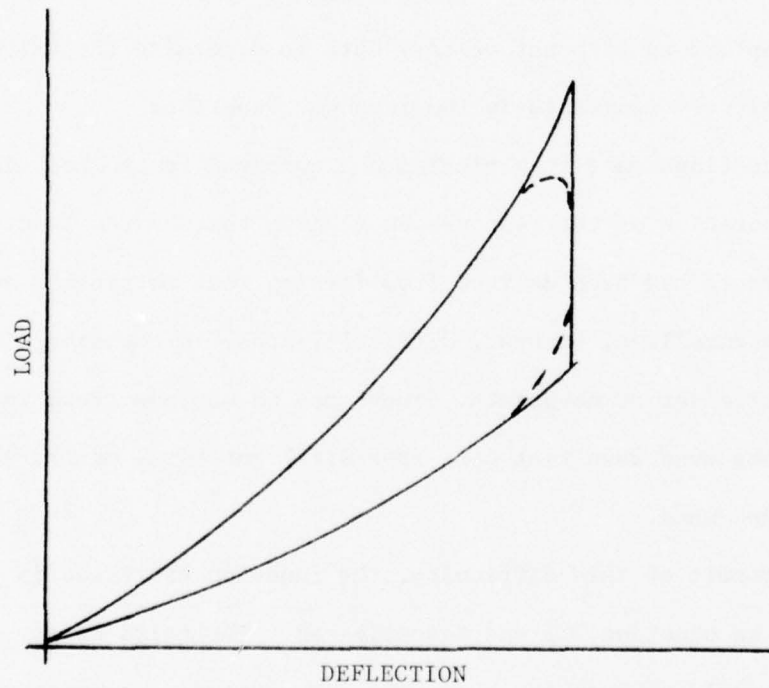


FIGURE 4.1 - RESPONSE TO TRIANGULAR LOAD PULSE

The arbitrary constants were again determined by using a least square fit of the data, and for this function there was a definite trend in the resulting numbers. Hence, it was decided to use equation 2.1 in the model, as was done in Chapter II. The problem then arose of just which set of constants to use, since there was variation in the actual numbers resulting from variations in the experimental results, which were discussed in Chapter III. It was decided to arbitrarily choose four tests, one for each ligament and at each loading rate, which gave numbers for the constants that were representative of the general trend. Tests 173 and 175 were chosen for the posterior longitudinal ligament and tests 184 and 185 were chosen for the anterior ligament. Table 4.1 shows the values of the constants derived from each set of test data, and the average values for the P.L.L. and A.L.L. which were used in the model. Figures 4.2 through 4.5 show the comparison between the fitted function and the actual test data. The functions plotted in these figures use the constants derived from that specific set of test data.

Table 4.1

Arbitrary Constants for Ligament Response Functions

	Test Nr.	A ₁	A ₂	A ₃	A ₄	A ₅
A.L.L.	184	2.37	541.91	17791.86	-22947.06	176.01
	185	2.51	437.51	18645.61	-26515.03	303.44
Average			489	18218	-24731	239
P.L.L.	173	7.94	1209.3	30350.37	-219646.08	190.76
	175	7.20	1153.68	21468.22	-200416.12	335.34
Average			1181	25909	-209831	262

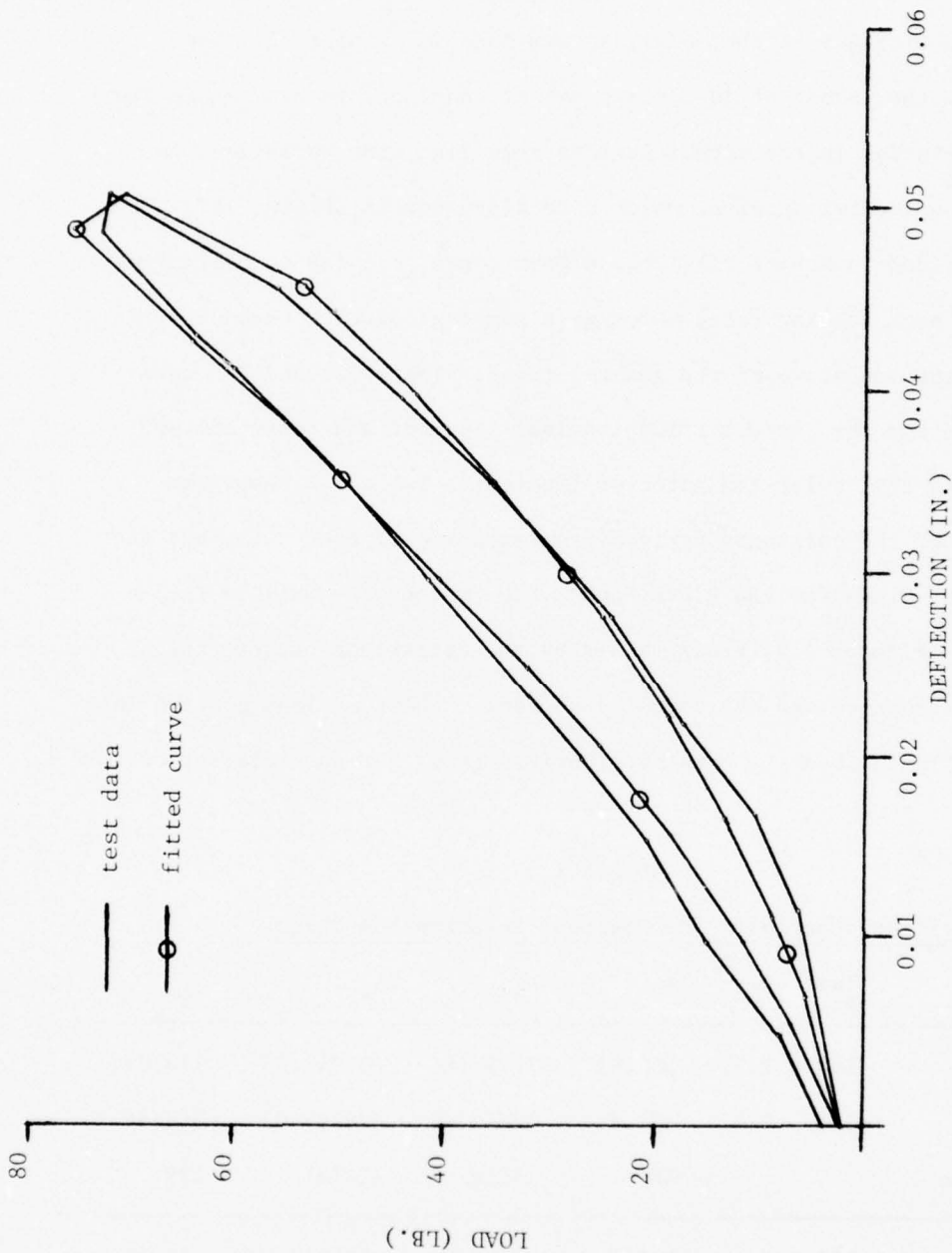


FIGURE 4.2 - LOAD VS. DEFLECTION -- TEST 184

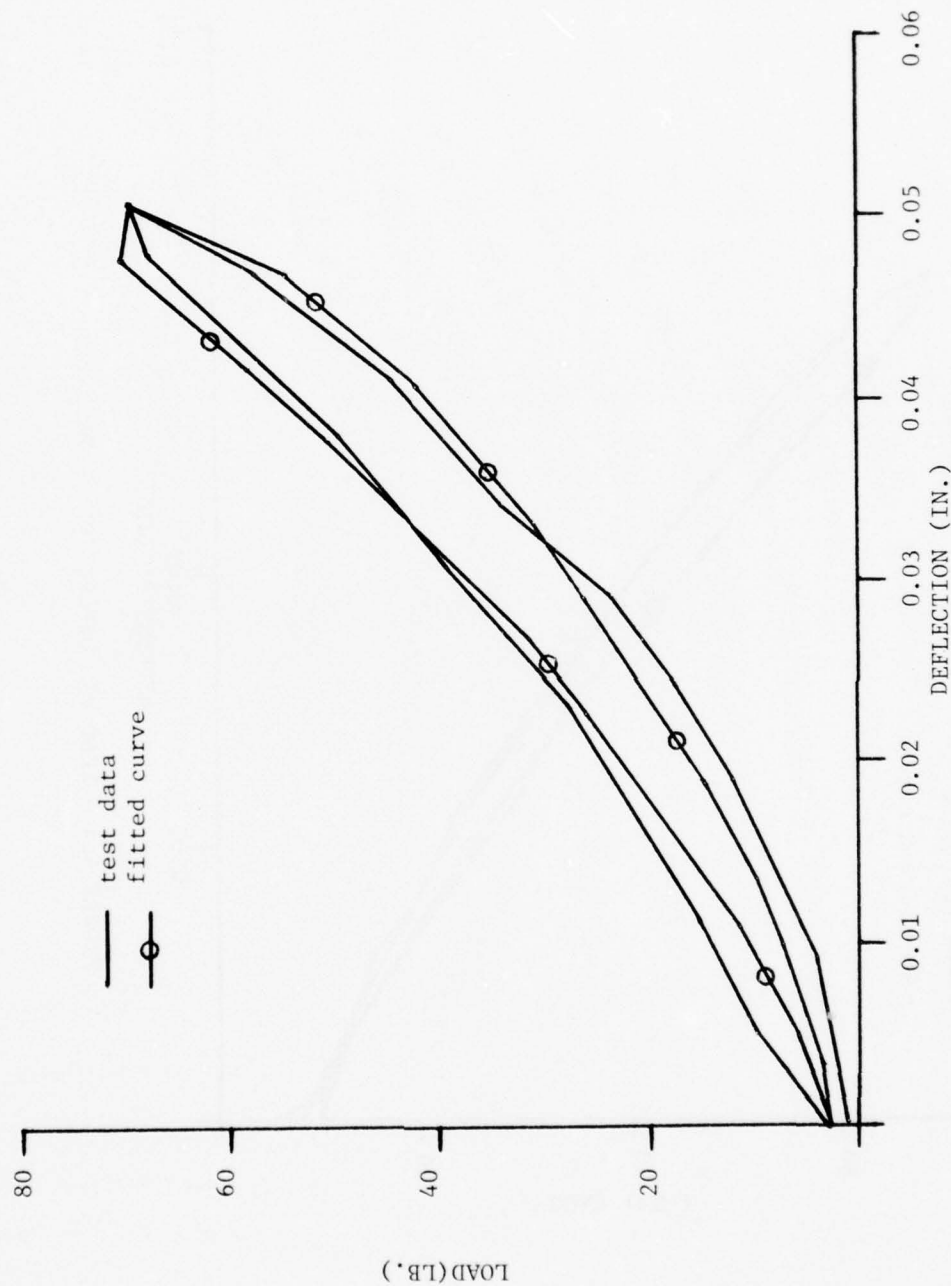


FIGURE 4.3 - LOAD VS. DEFLECTION -- TEST 185

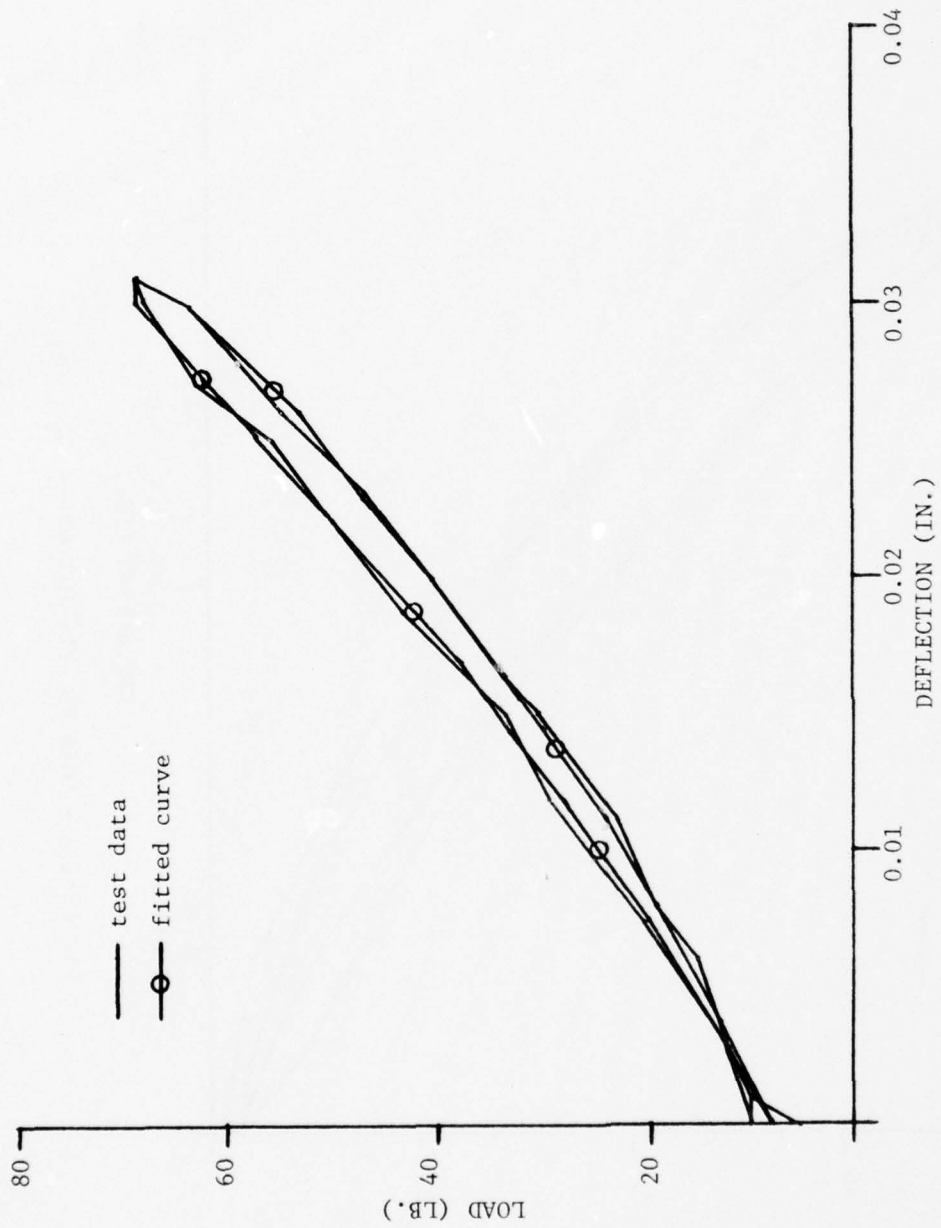


FIGURE 4.4 - LOAD VS. DEFLECTION -- TEST 173

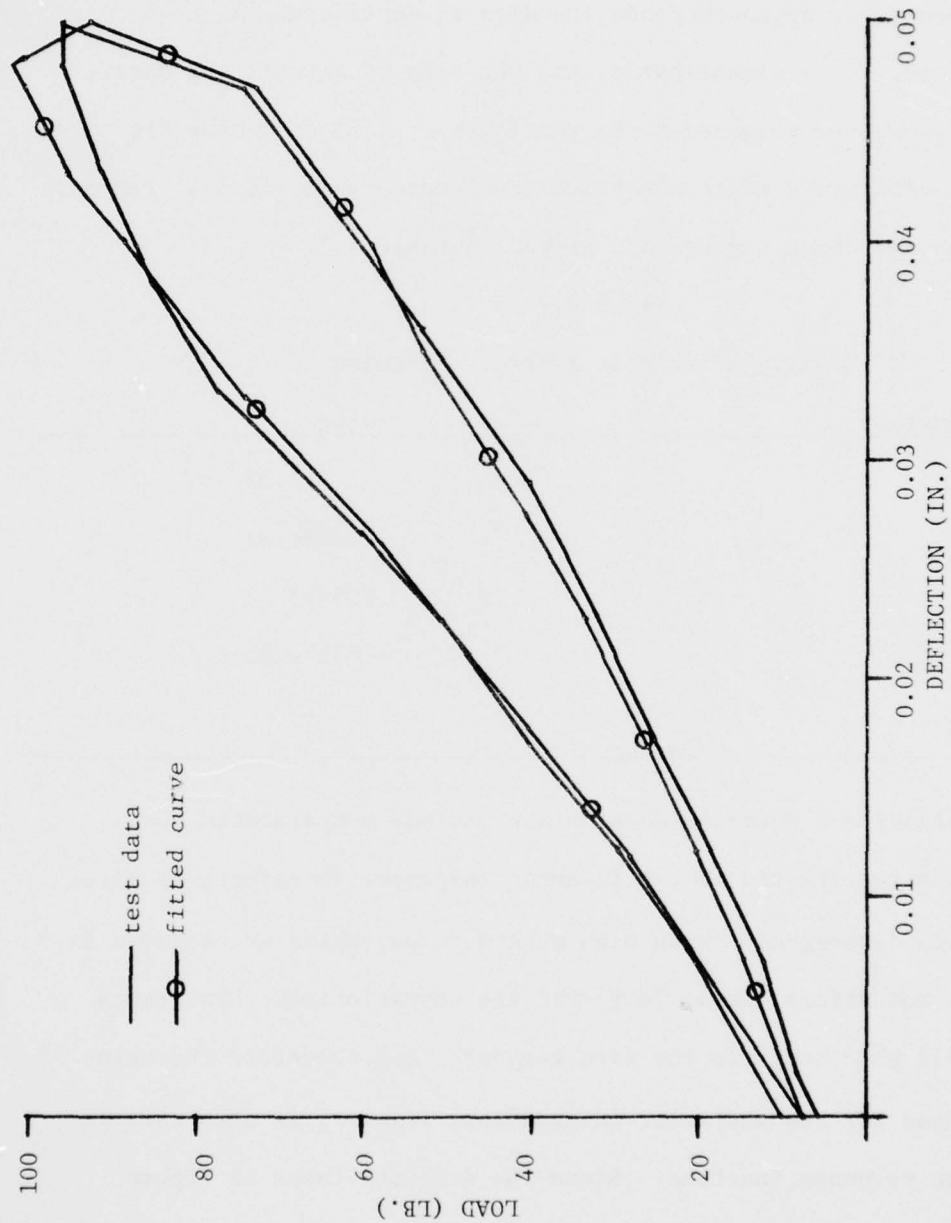


FIGURE 4.5 - LOAD VS. DEFLECTION -- TEST 175

The same function used for the ligaments is also used to characterize the response of the intervertebral disc. This was felt to be a reasonable approach since the disc is considered, in the literature, to be viscoelastic, and the data of Markolf and Morris (1974) show the response to be nonlinear. A least square fit of the data was used to establish the constants in the disc response function and those numbers are listed in table 4.2.

Table 4.2
Constants for Disc Response Function

Constant	Value
A ₁	7.52
A ₂	-434.23
A ₃	296913.79
A ₄	-768274.25
A ₅	-

Markolf and Morris's data do not include a hysteresis loop as was characteristic of the ligament response, therefore, no value for A₅ is determined. With high strain rates, which are assumed in the present effort, it is felt that the characteristic hysteresis loop will also occur in the disc response, and therefore the value of A₅ derived for the posterior longitudinal ligament is also used in the disc response function. Since the disc stiffness is higher than that of the ligaments, this should be a conservative constant for the velocity dependent term. When the function for the disc is input to the model in Chapter V, the constants are also adjusted to

account for the fact that they are based on data for the discs of the lower thoracic and lumbar spine. In this region of the spine, the discs are considerably larger than at the C7-T1 level, and a rationale for adjusting the values of the constants is provided in Chapter V.

CHAPTER V
PARAMETRIC RESULTS

5.1 Initial Solution.

In order to start the iterative solution discussed in Section 2.5, an initial guess must be made for the 31 variables. The values for the initial guess were determined by solving the static problem at time equal to zero.

The vertebra geometry and initial displacements were determined by measurements made on a lateral x-ray of the author's neck, and the application of the appropriate magnification factor to the measured values. These measurements required the fixing of the appropriate coordinate systems to the C7 and T1 vertebrae. Next, a contact point between the articulating facets was assumed and the position of that point was established. The x-ray does not clearly show the contact point, and therefore it had to be assumed. The variables x_{23} , y_{23} , x_{32} , y_{32} , γ and all the component displacements between the appropriate points on the two bodies are now known.

At this point, some assumptions had to be made. First a preload of 5.0 pounds was assumed in all the ligament elements of the model, and second, parabolic curves were assumed for the articulating facet surfaces. Also, a vertical load of 12 lb. and a moment of 8 in. lb. were applied to C7 to represent the static loads of the head and neck above C7. Data of Clauser et al. (1969) were used to make these estimates. With the known displacements, the components of forces F_5 , F_6 and F_7 can be determined as can the directions of F_3 , F_4 and F_8 . With these assumptions and the above geometric data, values for all the variables are known,

except M_2 and the magnitudes of F_3 , F_4 , F_8 , $F(1.2)$ and $F(2.2)$.

65

Values of these remaining values can be determined from a static force and moment balance.

Table 5.1 show the parameter for the first case investigated and Table 5.2 gives parameters for the second case. The second case is identical to the first except the angle α is rotated from -22° to -35° .

Table 5.1

Initial Conditions: -22°

$$\alpha = -22^\circ$$

$$F_5 = F_6 = F_7 = 5 \text{ lb.}$$

$$\delta = 0$$

$$F_8 = 6.843 \text{ lb.*}$$

$$F_3 = 9.257 \text{ lb.*}$$

$$M_3 = 8 \text{ in. lb.}$$

$$F_4 = 11.003 \text{ lb.*}$$

$$M_2 = -13.495 \text{ in.lb.}$$

* Calculated value

Table 5.2

Initial Conditions: -35°

$$\alpha = -35^\circ$$

$$F_5 = F_6 = F_7 = 5 \text{ lb.}$$

$$\delta = 0$$

$$F_8 = 6.2 \text{ lb.*}$$

$$F_3 = 7.531 \text{ lb.*}$$

$$M_3 = 8 \text{ in. lb.}$$

$$F_4 = 14.44 \text{ lb.*}$$

$$M_2 = 13.505 \text{ in.lb.*}$$

*Calculated values

The parameters listed in Table 4.1 were used in the function for the anterior and posterior longitudinal ligaments (F_5 and F_6). The posterior longitudinal ligament constants were doubled in the representation of ligament loads on the posterior arch and spinous process (F_7). The intervertebral disc elements were represented using the constants listed in Table 4.2; however, these values were adjusted based on disc cross sectional area data published by Yamada and Evans (1970). The ratio of the area of the cervical disc to the area of the discs from the lower thoracic and lumbar spine is 0.38. The constants in table 4.2 were multiplied by this factor, and then divided by two since the disc is represented by two loads in the model.

5.2 Velocity Effects.

Fig. 5.1 shows the loads and moments used as input to the model. In the first case where $\alpha = -22^\circ$, the model was run both with and without the $\dot{x}\ddot{x}$ term in the functional representation of the ligament and disc response.

Fig. 5.2, 5.3 and 5.4 show the results with and without the $\dot{x}\ddot{x}$ terms. There is very little change in the angle of rotation, but there is a marked difference in the relative motion between the articulating facet surfaces. These results demonstrate that the velocity dependence of the ligament and disc response does have a significant influence on the relative motion within the joint. It is surprising that the angle of rotation is not influenced more; however, it should be noted that the magnitude of the rotation is very small. This small angle of rotation is partly due to the assumption made when selecting the constants for F_7 , which represents the loads

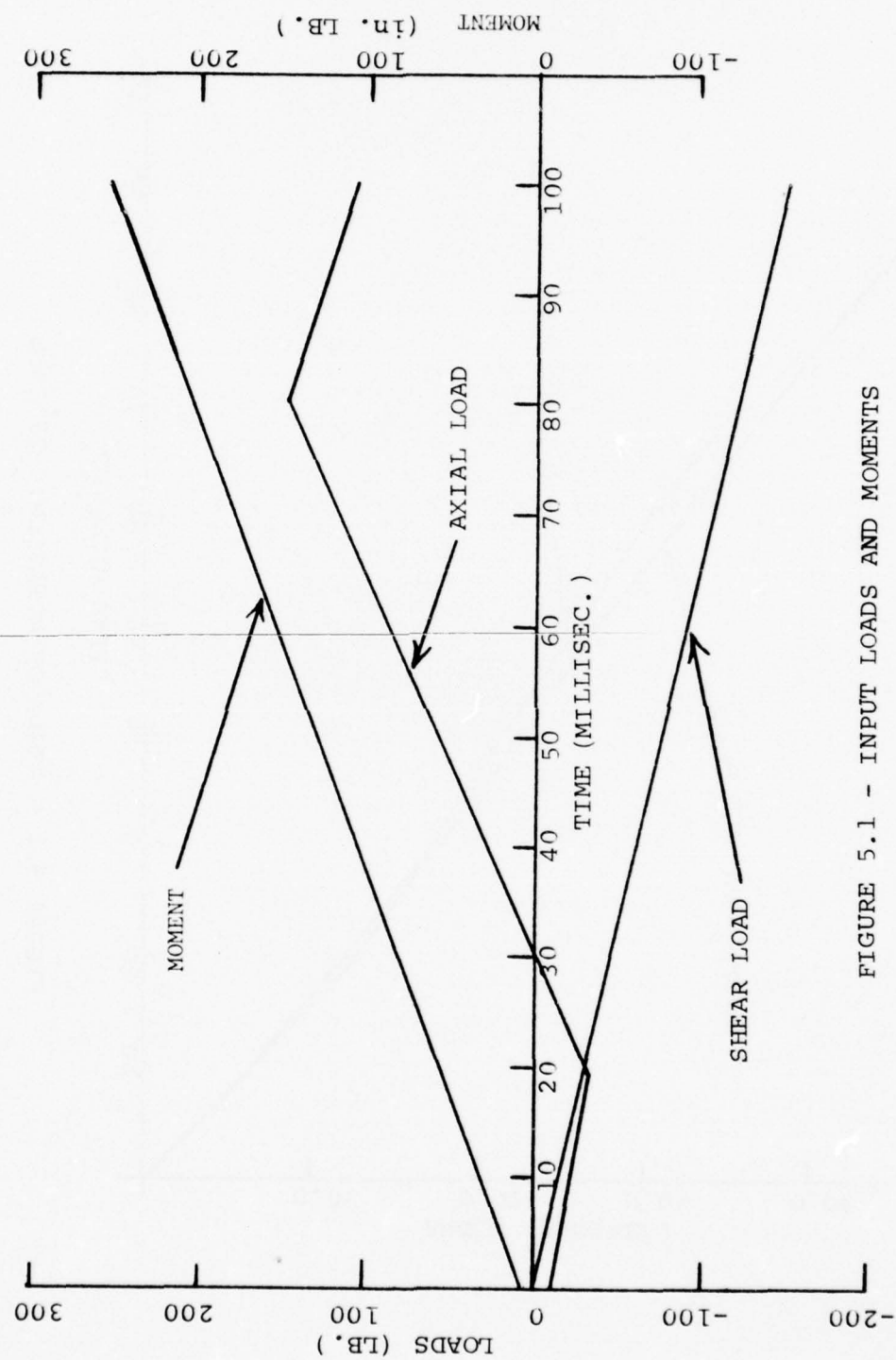


FIGURE 5.1 - INPUT LOADS AND MOMENTS

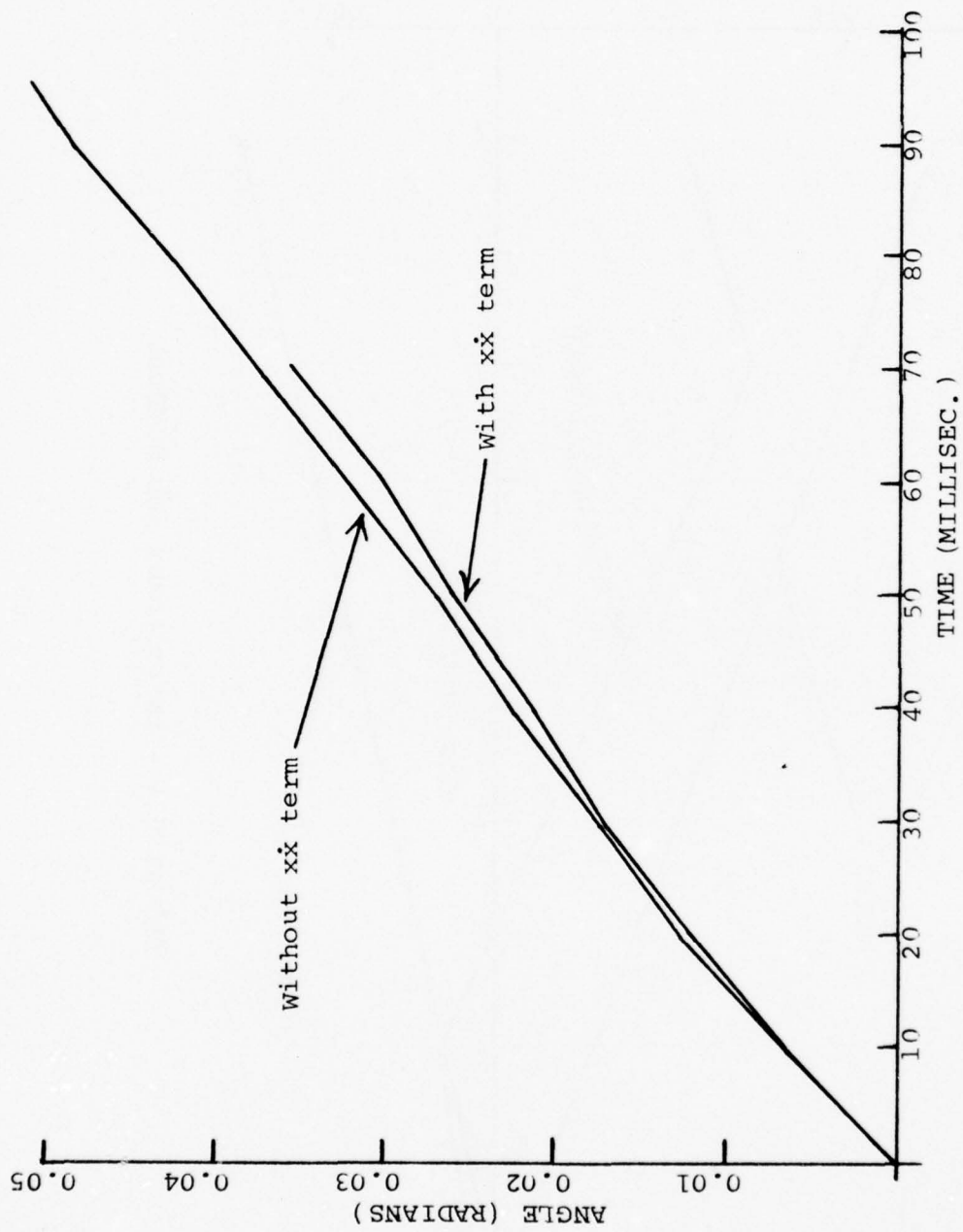


FIGURE 5.2 - ANGLE OF ROTATION: -22° CASE

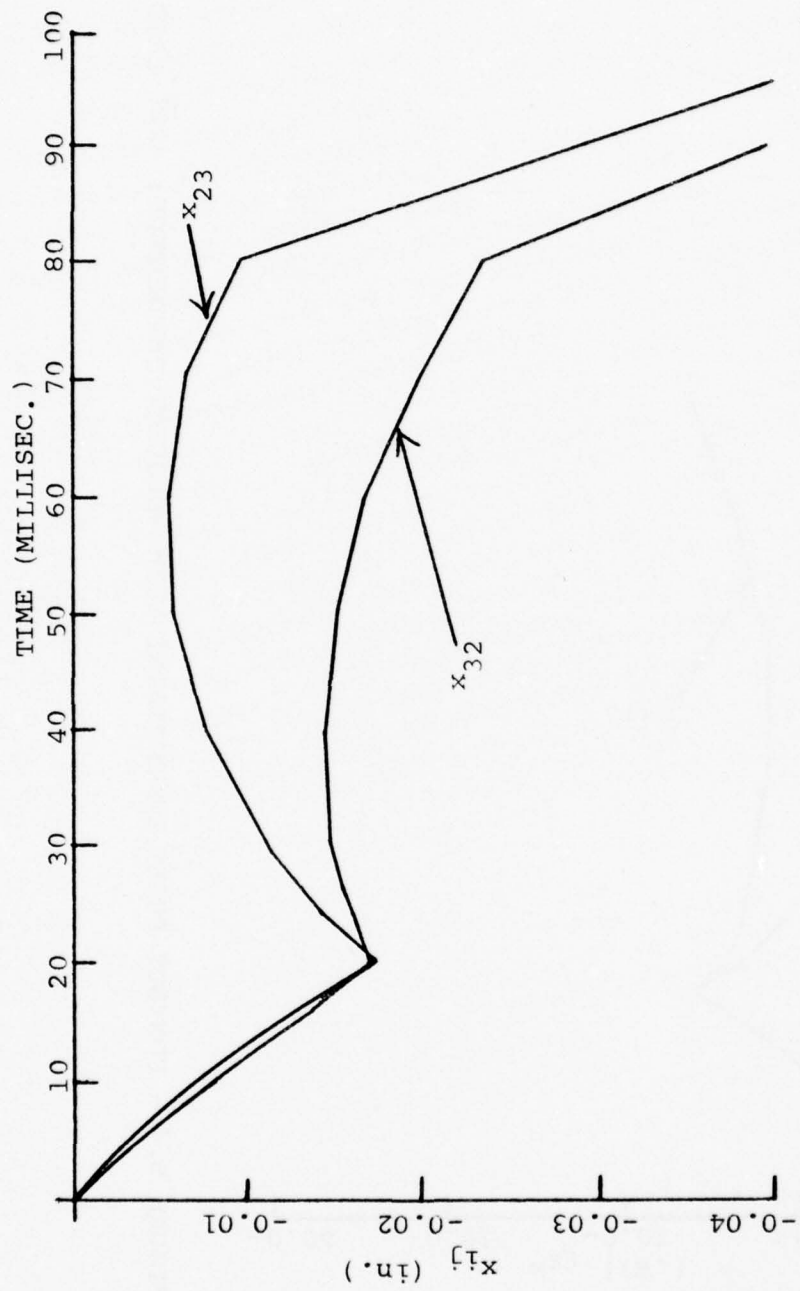


FIGURE 5.3 - CONTACT POINT COORDINATES WITHOUT VELOCITY DEPENDENCE: -22° CASE

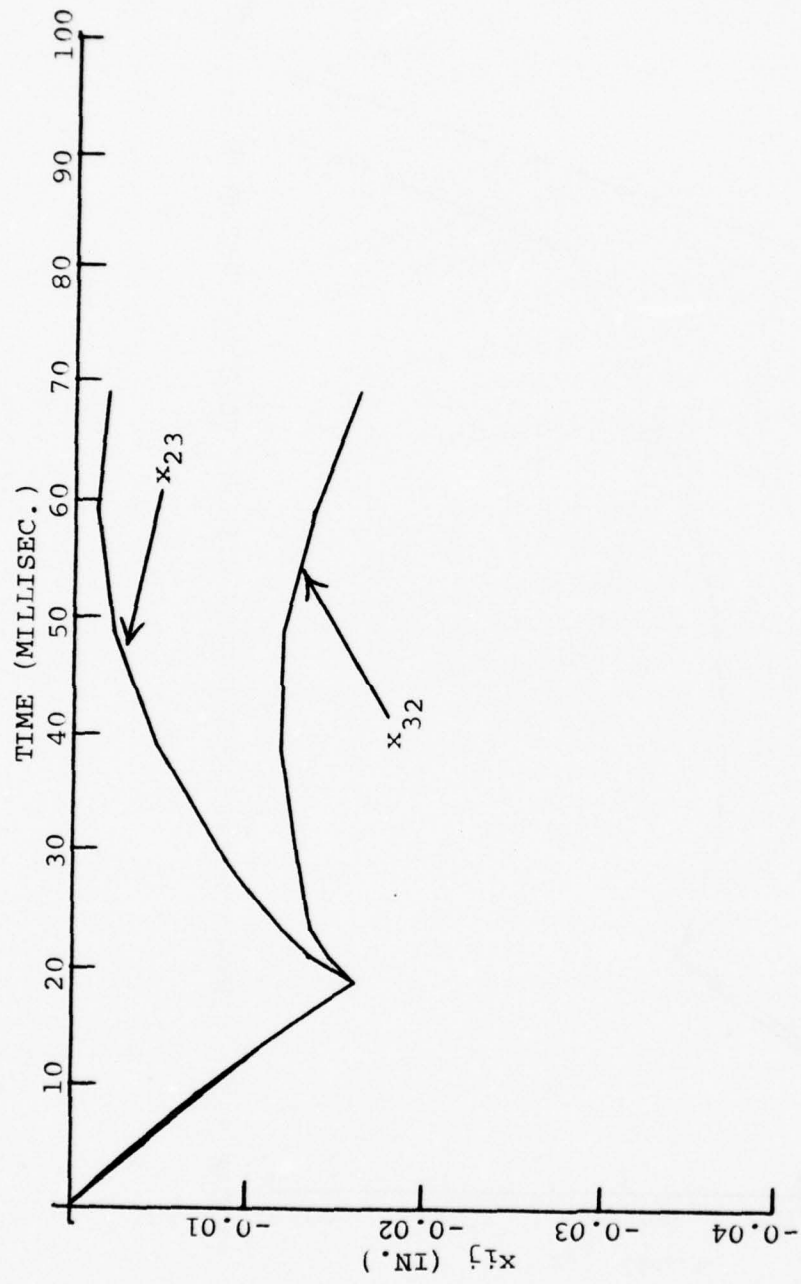


FIGURE 5.4 - CONTACT POINT COORDINATES WITH VELOCITY DEPENDENCE: -22° CASE

applied to the posterior portion of the vertebra. If the values of these constants for R_7 are too high, it could have a significant effect on the overall joint model. Therefore, the response of the ligaments of the posterior arch and spinous process remains an area requiring further investigation.

Note that the resulting velocities and displacements of the ligaments are similar in magnitude to those used in the experimental work discussed in Chapter III.

5.3 Articulating Facet Geometry Effect.

Figures 5.5 and 5.6 show results from the second case where α was rotated from -22° to -35° , and the constants for the velocity terms were set to zero. A comparison of Fig. 5.6 and 5.3 shows that the relative motion between the articulating surfaces is of the same general nature, i.e., the curve shapes are similar; however, the magnitude of the relative motion is greater in the -35° configuration. A comparison of Fig. 5.5 and Fig. 5.2 shows that the magnitude of the angle of rotation is again small. Up to 80 milliseconds the slope of the rotation angle vs. time plot for the -35° case is slightly steeper than in the -22° case, and both curves are nearly linear. At approximately 80 milliseconds the curve for the -35° case starts to flatten out which does not occur in the other case. This flattening of the curve would indicate that the more vertical orientation of the articulating facets tends to limit the angle of rotation. These results, along with the results discussed in section 5.2 above, demonstrate the ability of the model to predict variations in the joint motion as a function of geometric and material response parameters. Other parameters which could be investigated by the model would include the

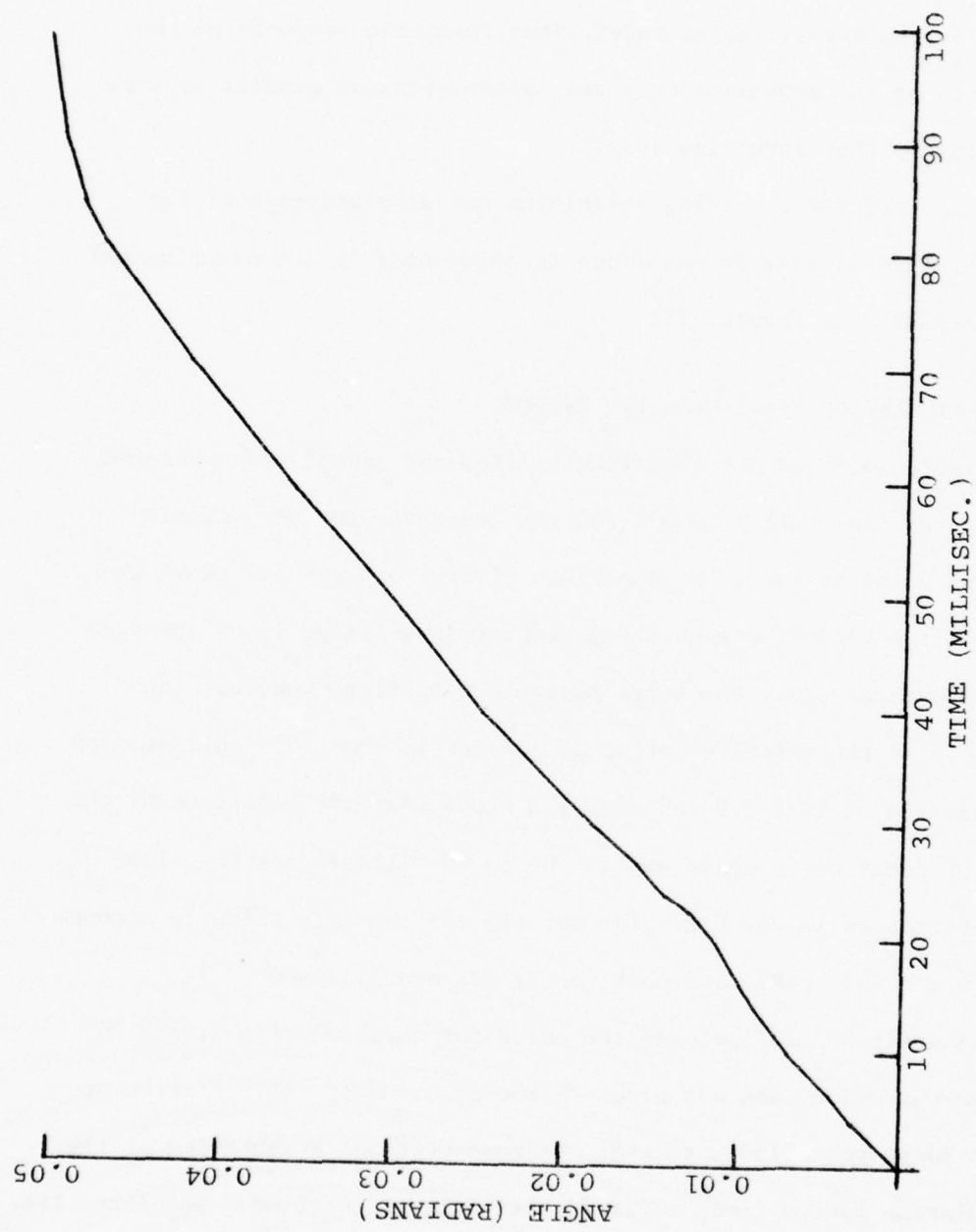


FIGURE 5.5 - ANGLE OF ROTATION: -35° CASE

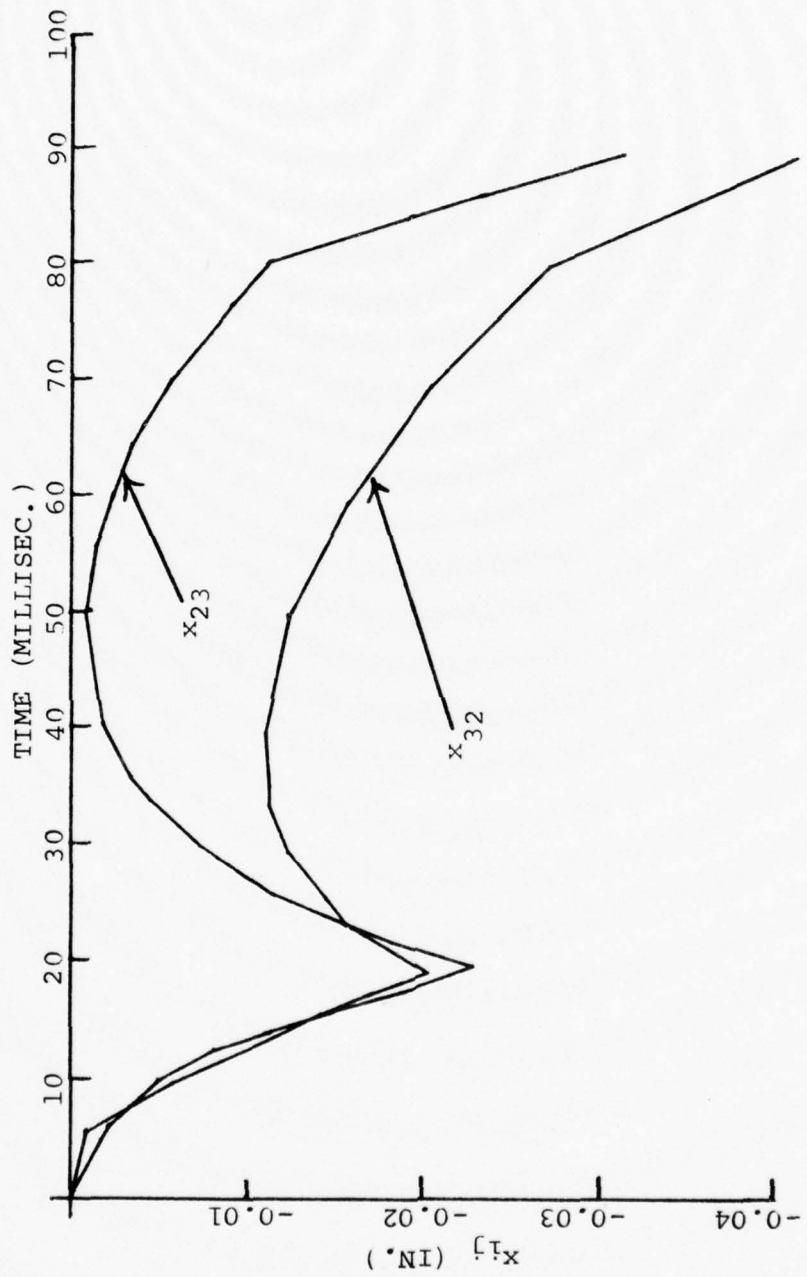


FIGURE 5.6 - CONTACT POINT COORDINATES: -35° CASE

input loads and moments, the shape of the articulating facet surfaces
and the functional representation of the ligament and disc response. 74

CHAPTER VI

CONCLUSIONS AND RECOMMENDATIONS

The work reported here demonstrates the feasibility of modeling the C7-T1 joint, incorporating the vertebra geometry and the material response characteristics of the various joint elements. The model provides the opportunity to investigate the joint response as a function of both geometric and material response parameters, as well as a function of the input loads and moments.

The parametric results reported are very limited, and in order to characterize the joint motion as a function of the various parameters, a more extensive parametric analysis is required. The limited results do indicate that the joint motion is significantly influenced by the joint geometry and also by the velocity dependent response of the ligaments.

The resulting motion predicted by the model is dependent on how well one can characterize the response of the various joint elements. Based on the experimental results, the function expressed as equation 2.1 along with the constants listed in table 4.1 characterize reasonably well, the response of the longitudinal ligaments. The experimental results only consider two loading velocities, 1.0 and 0.5 in./sec. Further experimental work is necessary to extend the characterization of the ligaments over a wider velocity range and to establish the velocity dependence of the response of the intervertebral discs and the posterior arch and spinous process ligaments.

In addition to better characterization of material response, the second area for improving the model would be to expand the present

two dimensional model to three dimensions. In a three dimensional model, surfaces rather than curves could be incorporated to realistically represent the articulating surfaces, and the asymmetries of the vertebrae could also be considered. The same kinematic constraint, as expressed by equation 2.2, would be used and the three dimensional model would be similar to the two dimensional model except the number of variables and the corresponding number of equations would increase.

The one influence on the joint motion which is not considered in the model is that of the muscles. Muscular influences were not included because of the difficulty of characterizing muscle response. A muscle response model, such as developed by Soechting and Mains (1971) or Crowe (1970), could have been incorporated in the model, but the muscular influences were considered to be beyond the scope of this effort.

Though only the C7-T1 joint is considered here, the model is not restricted to this one joint, and if desired, could be used to study other levels of the spinal column. This model or an analogous three dimensional model provides a useful tool for the parametric study of effects of the anatomical elements on the overall motion of the human vertebral joint.

APPENDIX A

Vector Between Points On Adjacent Vertebrae

The vector between points on adjacent vertebrae can be expressed as \vec{R}_{mn}^{lk} , where "l" is the inferior body, "k" is the superior body, and "m" and "n" are the points on the inferior and superior bodies respectively. Coordinates of points on the inferior body are in the (x_1, y_1) coordinate system, and points on the superior system are expressed in the (x_{kl}, y_{kl}) coordinate system.

Referring to Fig A.1, \vec{R} can be written in the vector equation as:

$$\vec{R}_{mn}^{lk} = \vec{r}_1 + \vec{r}_2 \quad (A.1)$$

where; \vec{r}_1 = vector from point (l,m) to the contact point between the vertebrae

\vec{r}_2 = vector from the contact point to point (k,n).

Vectors \vec{r}_1 and \vec{r}_2 are written:

$$\begin{aligned} \vec{r}_1 &= [-x(l,n) + x(l,2) + x_{lk} \cos \alpha - y_{lk} \sin \alpha] \hat{i}_l \\ &\quad + [-y(l,n) + y(l,2) + x_{lk} \sin \alpha + y_{lk} \cos \alpha] \hat{j}_l \end{aligned} \quad (A.2)$$

$$\vec{r}_2 = (-x_{kl} + x(k,n)) \hat{i}_{kl} + (-y_{kl} + y(k,n)) \hat{j}_{kl} \quad (A.3)$$

where; α = angle between coordinates fixed to the inferior body

$(x(1,2), y(1,2))$ = origin of the (x_{1k}, y_{1k}) coordinate system.

If γ is the angle between the (x_{1k}, y_{1k}) and the (x_{kl}, y_{kl}) coordinate systems, \vec{r}_2 can be express as:

$$\begin{aligned} \vec{r}_2 &= [(-x_{kl} + x(k,n)) \cos(\alpha + \gamma) \\ &\quad + (-y_{kl} + y(k,n)) (-\sin(\alpha + \gamma))] \hat{i}_l \end{aligned} \quad (A.4)$$

$$+ \left[(-x_{kl} + x(k,n)) \sin(\alpha + \gamma) \right. \\ \left. + (-y_{kl} + y(k,n)) \cos(\alpha + \gamma) \right] \vec{f}_k$$

Substituting equations A.2 and A.4 into equation A.1 gives:

$$\begin{aligned} \vec{R}_{mn}^{lk} = & \left[-x(l,m) + x(l,2) + x_{lk} \cos \alpha - y_{lk} \sin \alpha \right. \\ & + (x(k,n) - x_{kl}) \cos(\alpha + \gamma) - (y(k,n) - y_{kl}) \sin(\alpha + \gamma) \left. \right] \vec{i}_l \\ & + \left[-y(l,m) + y(l,2) + x_{lk} \sin \alpha + y_{lk} \cos \alpha \right. \\ & \left. + (x(k,n) - x_{kl}) \sin(\alpha + \gamma) + (y(k,n) - y_{kl}) \cos(\alpha + \gamma) \right] \vec{f}_l \end{aligned} \quad (\text{A.5})$$

This is the same equation as equation 2.5 in Chapter II. If the small angle approximation is used for γ , then $\sin(\alpha + \gamma)$ and $\cos(\alpha + \gamma)$ become $(\sin \alpha + \gamma \cos \alpha)$ and $(\cos \alpha - \gamma \sin \alpha)$, respectively.

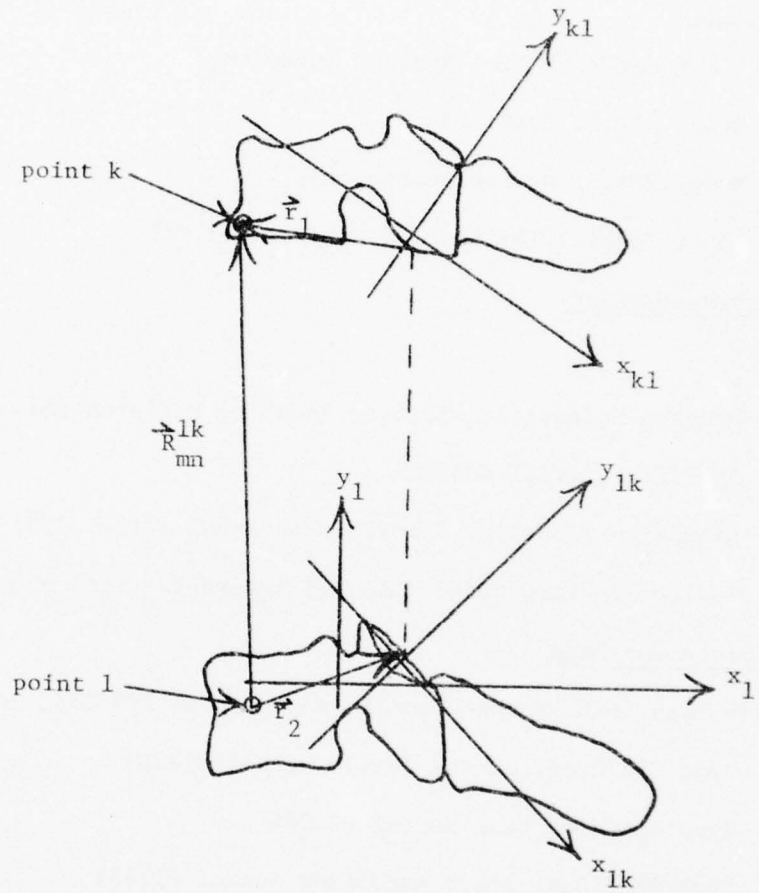


FIGURE A.1 - VECTOR \vec{R}_{mn}^{1k}

APPENDIX B

Test Equipment

Loading Apparatus

MTS Model 810 Material Test System, Including:

- a. Model 311.21 Test Frame
- b. Model 204.51 Hydraulic Actuator
- c. Lebow Model 3116-103 Load Cell Serial 986

Recording Instrumentation

Load Data

- a. Preston Scientific Wideband Floating Differential Amplifier Serial ACA693
- b. Biomation Transient Recorder Model 802 Serial 1621
- c. Hewlett-Packard Model 136A X-Y Recorder Serial 820-01235

Load and Displacement Data

Tektronix Type 564B Storage Oscilloscope Serial B090125, Including:

- a. Type C12 Oscilloscope Camera Serial 018315
- b. Type 3B4 Time Base Serial 005386
- c. Type 3A72 Dual Trace Amplifier Serial 011431

APPENDIX C

Test Parameters

Test Number	e* (in.)	t* (m. sec.)	(Pre-stress) (lb.)	Initial Set** (in.)
111	0.10	100	22	0.177
112	0.10	100	3.9	"
113	0.10	100	2.4	"
114	0.10	300	1.7	"
115	0.10	300	0.0	"
116	0.10	100	0	"
117	0.10	100	3.7	0.195
118	0.15	100	3.9	0.200
121	0.10	100	6.3	"
122	0.10	100	6.8	"
123	0.10	100	4.5	"
124	0.10	100	4.2	"
125	0.10	300	3.9	"
126	0.10	300	4.0	"
127	0.10	50	4.1	"
128	0.10	50	3.8	"
131	0.10	100	6.8	0.103
132	0.10	100	7.4	0.12
133	0.10	100	5.0	"
134	0.10	100	3.0	"
135	0.10	100	0	"
136	0.10	300	0	"
137	0.10	300	0	"
141	0.10	100	8.1	"

* For definition, see Fig. 3.1.

** The initial set is equal to the thickness of the lips on the test fixture (0.14 in.) plus the separation between the halves of the fixture before the test.

Test Number	e* (in.)	t* (m. sec.)	(Pre-stress) (lb.)	Initial Set** (in.)
142	0.05	100	0	0.144
143	0.05	100	0	"
144	0.10	100	0	"
145	0.10	100	0	"
146	0.10	100	0	"
147	0.10	300	0	"
148	0.10	300	0	"
151	0.05	50	7.9	0.110
152	0.05	50	3.6	"
153	0.05	50	2.7	"
154	0.05	100	2	"
156	0.06	60	2	"
157	0.06	60	2	"
158	0.06	120	1	"
159	0.07	70	1	"
160	0.07	140	1	"
161	0.08	80	1	"
162	0.08	160	1	"
163	0.05	50	1	"
164	0.10	100	1	"
165	0.50	50	1	"
166	0.10	100	1	"
171	0.03	30	9.3	0.140
172	0.03	30	9.9	"
173	0.03	60	9.6	"
174	0.03	60	11.4	0.142

Test Number	e* (in.)	t* (m.sec.)	(Pre-stress) (1b.)	Initial Set** (in.)
175	0.05	50	10.6	0.142
176	0.05	100	8.2	"
177	0.05	30	7.9	"
178	0.03	30	7.6	"
179	0.10	100	7.5	"
181	0.03	300	6.3	0.159
182	0.03	30	4.1	"
183	0.03	60	3.8	"
184	0.05	50	3.5	"
185	0.05	100	2.8	"
186	0.07	70	2.3	"
187	0.07	140	1.5	"
188	0.10	100	1	"
191	0.03	30	48.4	0.142
192	0.03	60	34.8	"
193	0.05	50	30.4	"
194	0.05	100	21.8	"
195	0.05	100	19.1	"
196	0.10	100	16.6	"
201	0.03	30	4.5	0.163
202	0.03	60	2.7	"
203	0.05	50	2.5	"
204	0.10	200	0	"
211	0.03	30	9.5	0.142
212	0.03	60	7.0	"
213	0.05	50	6.6	"

<u>Test Number</u>	<u>e*</u> (in.)	<u>t*</u> (m.sec.)	<u>(Pre-stress)</u> (1b.)	<u>Initial Set**</u> (in.)	⁸⁴
214	0.05	100	4.6	0.142	
215	0.07	70	4.0	"	
216	0.07	140	2.8	"	
217	0.10	100	2.4	"	

REFERENCES

1. Akerblom, Bengt. Standing and Sitting Posture. Translated by Ann Synge. Stockholm: A.-B. Nordiska Bokhandeln, 1948.
2. Bhalla, S.K., and E.M. Simmons. "Normal Ranges of Intervertebral-Joint Motion of the Cervical Spine". Canadian Journal of Surgery, Volume 12 (1969).
3. Clarke, T.D., C.D. Gragg, J.F. Sprouffske, E.M. Trout, R.M. Zimmerman, and W.H. Muzzy. "Human Head Linear and Angular Acceleration During Impact". Fifteenth Stapp Car Crash Conference, 1971.
4. Clauser, Charles E., John T. McConville, and J.W. Young. Weight, Volume and Center of Mass of the Human Body. AMRL-TR-69-70 (AD 710622), Aerospace Medical Research Laboratory, Wright-Patterson Air Force Base, Ohio, 1969.
5. Clemens, H.J. and K. Burow. "Experimental Investigation on Injury Mechanics of Cervical Spine at Frontal and Rear-Front Vehicle Impacts". Sixteenth Stapp Car Crash Conference, 1972.
6. Crowe, Alan. "A Mechanical Model of Muscle and Its Application to the Intrafusal Fibers of the Mammalian Muscle Spindle". Journal of Biomechanics, Volume 3 (1970).
7. Culver, C.C., R.F. Neathery, and H.J. Mertz. "Mechanical Necks and Humanlike Responses". Sixteenth Stapp Car Conferences, 1972.
8. Farfan, H.F. "The Relationship of Facet Orientation to Intervertebral Disc Failure". The Canadian Journal of Surgery, Volume 10 (1967).
9. Farfan, H.F. "Effects of Torsion on the Intervertebral Joints". The Canadian Journal of Surgery, Volume 12 (1969).
10. Flugge, Wilhelm. Viscoelasticity. Blaisdell Publishing Company, Waltham, Mass. (1967).
11. Fung, Y.C., N. Perrone and M. Anleker, Editors. Biomechanics, Its Foundations and Objectives. Englewood Cliffs, Prentice Hall, Inc., 1972.
12. Godd, C.W., C.C. Culver, and A.M. Naham. "A Study of Responses and Tolerances of the Neck". Fifteenth Stapp Car Crash Conference, 1971.
13. Gray, Henry. Anatomy of the Human Body. Edited by Charles Moyn Goss. Philadelphia: Lea and Febiger, 1973.

14. Hamming, Richard W. and E.A. Feigenbaum. Introduction to Applied Numerical Analysis. New York: McGraw-Hill Book Company, 1971.
15. Hopkins, G. R., "Nonlinear Lumped Parameter Mathematical Model of the Dynamic Response of the Human Body" in Symposium on Biodynamic Models and Their Applications. AMRL-TR-71-29 (AD 739501), Aerospace Medical Research Laboratory, Wright-Patterson AFB, OH, 1971.
16. Ingelmark, B.E., "Function of the Pathological Changes in Spinal Joints". Acta Anatomica, Supplement 36 (1959).
17. Kazarian, Leon. "Dynamic Response Characteristics of the Human Vertebral Column". Acta Orthop. Scand. Supplement 146 (1972).
18. Kazarian, Leon, Dale D. Boyd and Henning E. von Gierke. The Dynamic Biomechanical Nature of Spinal Fractures and Articular Facet Derangement. AMRL-TR-71-17 (AD 731148), Aerospace Medical Research Laboratory, Wright-Patterson Air Force Base, Ohio, 1971.
19. Kazarian, Leon. Personal Communication, July 1974.
20. Krause, H. E. and M. Shirazi. "The Transverse Response of the Lumbar Spine Under Longitudinal Loads" in AMRL-TR-71-29 (AD 739501), Aerospace Medical Research Laboratory, Wright-Patterson AFB, Ohio, 1971.
21. Lange, W. "Mechanical and Physiological Response of the Human Cervical Vertebral Column to Severe Impacts Applied to the Torso" in AMRL-TR-71-29 (AD 739501), Aerospace Medical Research Laboratory, Wright-Patterson AFB, Ohio, 1971
22. Li, T. F., S. H. Advani, and Y. C. Lee. "The Effect of Curvature on the Dynamic Response of the Spine to Axial Acceleration" in AMRL-TR-71-29 (AD 739501), Aerospace Medical Research Laboratory, Wright-Patterson AFB, Ohio, 1971.
23. Liu, Y. King, J. Monroe Laborde and W.C. Von Buskirk. "Inertial Properties of a Segmented Cadaver Trunk: Their Implications in Acceleration Injuries". Aerospace Medicine. Volume 42 (June 1971)
24. Moins, R.E., and J.F. Soechting. "A Model for the Neuromuscular Response to Sudden Distrubances". Journal of Dynamic Systems, Measurements and Control, Volume 93, No. 4 (1971)
25. Markolf, Keith L., and James M. Morris. "The Structural Components of the Intervertebral Disc". Journal of Bone and Joint Surgery, Volume 56-A, No. 4. (June 1974).

26. McCracken, Daniel D., and William S. Dorn. Numerical Methods and Fortran Programming. New York: John Wiley and Sons, 1964.
27. Melvin, John W., James H. McElhaney, and Verne L. Roberts. "Improved Neck Simulation for Anthropometric Dummies". Sixteenth Stapp Car Crash Conference, 1972.
28. Mertz, H.J., and L.M. Patrick. "Strength and Response of the Human Neck". Fifteenth Stapp Car Crash Conference, 1971.
29. Nachemson, A. "Lumbar Interdiscal Pressure". Acta Orthop. Scand., Supplement 43 (1960).
30. Nachemson, A. "The Influence of Spinal Movement on the Lumbar Interdiscal Pressure and on the Tensile Stresses in the Annulus Fibrosus". Acta Orthop. Scand., Col. 33-183 (1963).
31. Nachemson, Alf L., and John H. Evans. "Some Mechanical Properties of the Third Human Lumbar Interlaminar Ligament (Ligamentum Flavum)". Journal of Biomechanics, Volume 1 (1968).
32. Orne, David, and Y. King Liu. "A Mathematical Model of Spinal Response to Impact". Journal of Biomechanics, Volume 4, (1971).
33. Rybicki, E. F. and A. T. Hopper. "A Dynamic Model of the Spine Using a Porous Elastic Material" in AMRL-TR-71-29 (AD 739501), Aerospace Medical Research Laboratory, Wright-Patterson Air Force Base, Ohio, 1971.
34. Shirazi, M. "Response of the Spine to Biodynamic Environments" in AMRL-TR-71-29 (AD 739501), Aerospace Medical Research Laboratory, Wright-Patterson Air Force Base, Ohio, 1971.
35. Soechting, John F., and Paul R. Pasley. "A Model for the Human Spine During Impact Including Musculature Influence". Journal of Biomechanics, Volume 6, No. 2 (1973).
36. Thurston, Gayland A., and Richard J. Foy. "Theoretical and Mechanical Models of the Human Neck". Final Report, Contract Number N000 14-67-A-0394-003, Office of Naval Research, June 1974.
37. Tkaczuk, H. "Tensile Properties of Human Lumbar Longitudinal Ligaments". Acta Orthop. Scand. Supplement 115 (1968).
38. Toth, R. "Multiple Degree of Freedom Nonlinear Spinal Model". Nineteenth Annual Conference of Engineering in Medicine and Biology, 1967.

39. Yamada, H., and F.G. Evans. Strength of Biological Materials.
The Williams and Wilkins, Company, 1970.